Analysis and Modeling of Airport Surface Operations

by

Harshad Khadilkar

Submitted to the Department of Aeronautics and Astronautics
in partial fulfillment of the requirements for the degree of

Master of Science in Aeronautics and Astronautics

at the

MASSACHUSETTS INSTITUTE OF TECHNOLOGY

June 2011

Author .....
Department of Aeronautics and Astronautics
May 07, 2011

Certified by .....
Hamsa Balakrishnan
Assistant Professor of Aeronautics and Astronautics
Thesis Supervisor

Accepted by .....
Eytan H. Modiano
Associate Professor of Aeronautics and Astronautics
Chair, Graduate Program Committee

Analysis and Modeling of Airport Surface Operations

by

Harshad Khadilkar

Submitted to the Department of Aeronautics and Astronautics
on May 07, 2011, in partial fulfillment of the
requirements for the degree of
Master of Science in Aeronautics and Astronautics

Abstract

The focus of research in air traffic control has traditionally been on the airborne flight phase. Recently, increasing the efficiency of surface operations has been recognized to have significant potential benefits in terms of fuel and emissions savings. To identify opportunities for improvement and to quantify the consequent gains in efficiency, it is necessary to characterize current operational practices. This thesis describes a framework for analysis of airport surface operations and proposes metrics to quantify operational performance. These metrics are then evaluated for Boston Logan International Airport using actual surface surveillance data. A probabilistic model for real-time prediction of aircraft taxi-out times is described, which improves upon the accuracy of previous models based on queuing theory and regression. Finally, a regression model for estimation of aircraft taxi-out fuel burn is described. Together, the modules described here form the basis for a surface operations optimization tool that is currently under development.

Thesis Supervisor: Hamsa Balakrishnan
Title: Assistant Professor of Aeronautics and Astronautics

Acknowledgments

The authors would also like to acknowledge regular inputs provided by Prof. John Hansman, Dr. Richard Jordan, Dr. Mariya Ishutkina and Dr. Tom Reynolds from MIT/Lincoln Laboratory and Brendan Reilly from the FAA. In addition, we also thank Jim Eggert and Daniel Herring from MIT Lincoln Laboratory for their help with setting up the ASDE-X data transfer process.

On a personal note, I would like to acknowledge the able guidance, ideas and motivation provided by my advisor Prof. Hamsa Balakrishnan. A big thank you goes out to all my ICAT colleagues, in particular Ioannis Simaiakis, Varun Ramanujam, Diana Michalek-Pfeil, Hanbong Lee, Juan Jose Rebollo, Alex Donaldson and Lishuai Li for constant feedback and suggestions. Specifically, parts of Chapter 3 were worked on in close collaboration with Ioannis Simaiakis. Last but not least, I thank my parents, family and friends for their continued support, advice and encouragement.

Contents

List of Figures

List of Tables

Nomenclature

ASDE-X	Airport Surface Detection Equipment, Model-X
ASPM	Aviation System Performance Metrics
ASQP	Airline Service Quality Performance system
MMF	Multi-Modal (Unscented Kalman) Filter
UKF	Unscented Kalman Filter
ICAO	International Civil Aviation Organization
FDR	Flight Data Recorder
MTOW	Maximum TakeOff Weight
X	Position (meters east)
Y	Position (meters north)
V	Taxi speed (m/s)
θ	Heading (degrees)
a_f	Acceleration value (m/s^2) in process model of filter f
ω_f	Turn rate value (deg/s) in process model of filter f
$\bar{w}$	Process noise
$\bar{v}$	Measurement noise
σ^2_{wA}	Assumed process noise variance of quantity A
σ^2_{vA}	Assumed measurement noise variance of quantity A
P	Sigma point generator matrix
Q	Process noise covariance matrix
Q_d	Discrete equivalent process noise covariance matrix
R	Measurement noise covariance matrix
$w_{c,i}$	Sigma-point weights for covariance update
$w_{m,i}$	Sigma-point weights for mean update
$\hat{\bar{x}}$	Estimated state vector
$\bar{y}$	Actual measurement vector
$\hat{\bar{y}}$	Estimated measurement vector
$\bar{x}^{(i)}$	i^{th} sigma point
T_s	Measurement time step
T_{amb}	Ambient temperature
f	Total fuel consumed during taxi-out
t	Taxi-out time
n_s	Number of stops
n_t	Number of turns
n_a	Number of acceleration events

Chapter 1

Introduction

1.1 Motivation

The field of air transportation has been a topic of intense research in recent years. The focus of this scrutiny has been on the financial aspects of the airline industry, the alleviation of delays to passengers, more efficient air traffic control procedures, and aircraft fuel burn and emissions. Efficient surface operations are a relatively new field of interest. However, there is increasing awareness of the significant benefits that research in this area can offer. Departure operations at airports are the most susceptible to delay, due to downstream constraints in the airspace, and stand to benefit the most from improved procedures and technologies. Therefore, in this thesis, we have tried to develop a picture of the current state of airport surface operations in general, and taxi-out procedures in particular. In order to truly understand the departure process, it is necessary to have access to detailed data relating to aircraft operations. Traditionally, such data has been available for airborne operations, but not for surface operations. Fortunately, the recent introduction of surface surveillance equipment such as the Airport Surface Detection Equipment, Model-X (ASDE-X) [1] in major US airports (29 as of November 2010) has solved this problem. We were able to access this data through the MIT Lincoln Laboratory's Runway Status Lights system. A major part of this thesis will focus on leveraging archived ASDE-X data for analysis of surface operations and for prediction of aircraft behavior on the ground.

1.2 Thesis Development

While ASDE-X data offers tremendous opportunities for development of efficient procedures and assessment of potential benefits, it comes with its own challenges. The detailed nature of the data means that archived files are large, with each day's data occupying approximately 2GB of disk space. Therefore, identifying and sorting individual flight tracks is difficult. This is further complicated by exogenous tracks in the data, which may be produced by helicopters, aircraft being towed, or ground vehicles with transponders. Finally, the raw data also contains a large amount of noise. This means that a large amount of preprocessing is required before the surface surveillance data can be used for further analysis.

Consequently, Chapter 2 describes a multi-modal Unscented Kalman Filter developed for estimation of aircraft position, velocity and heading from noisy surface surveillance data. The raw data is composed of tracks generated by the Airport Surface Detection Equipment, Model-X at Boston Logan International Airport. The multi-modal filter formulation facilitates estimation of aircraft taxi mode, described by different acceleration and turn rate values, in addition to aircraft states. The resulting sorted and smoothed flight tracks are used for the analysis described in the two subsequent chapters.

Chapter 3 describes how airport performance characteristics such as departure queue dynamics and throughput can be measured using surface surveillance data. Several metrics to measure the daily operational performance of an airport are also proposed and evaluated. The results presented are for the specific case of Boston Logan International Airport.

The accurate prediction of aircraft taxi-out times is the first step toward the optimization of departure operations at airports. In Chapter 4, we present a taxi-out time prediction tool that models the airport surface as a network. Travel times along links of the network are assumed to be random variables with unknown distributions. The methodology used to derive these distributions from empirical surface surveillance data is described. The resulting theoretical model is validated using observations from

an independent test data set, and is shown to predict taxi-out times accurately. The resultant airport surface model lends itself to use with existing route optimization algorithms with minor modifications.

In addition to ASDE-X data, we also had access to a limited amount of Flight Data Recorder (FDR) data. In addition to position and velocity, this data set also contains information on instantaneous fuel flow rate. Chapter 5 uses the FDR data to build a model for estimation of on-ground fuel consumption of an aircraft, given its surface trajectory. This model is an important part of any procedure that optimizes departure operations as it allows the assessment of potential fuel savings. Since the taxi-out phase of a flight accounts for a significant fraction of total fuel burn for aircraft, reduced taxi-out times will result in reduced CO_2 emissions in the vicinity of airports. In Chapter 5, taxi-out fuel burn is modeled as a linear function of several factors including the taxi-out time, number of stops, number of turns, and number of acceleration events. The parameters of the model are estimated using least-squares regression. The statistical significance of each of these factors is investigated. Since these factors are estimated using data from operational aircraft, they provide more accurate estimates of fuel burn than methods that use idealized physical models of fuel consumption based on aircraft velocity profiles, or the baseline fuel consumption estimates provided by the International Civil Aviation Organization. Our analysis shows that in addition to the total taxi time, the number of acceleration events is a significant factor in determining taxi fuel consumption.

Finally, Chapter 6 describes a method for applying the model to the estimation of fuel burn for flight tracks generated from surface surveillance data. A procedure that could be used to estimate fuel burn benefits from congestion management strategies is also suggested. Chapter 7 summarizes the important findings in this thesis, and suggests directions for future work.

Chapter 2

ASDE-X Data Preprocessing

The two sets of data (ASDE-X and FDR) used in this work are in time-series format. At every time step, individual aircraft states are reported. Sorting and concatenating several successive reports from the same aircraft generates flight tracks. However, the tracks thus generated contain a significant proportion of noise. Therefore, both sets of data require filtering. The noise content in FDR data is fairly low, since all the states are measured using onboard equipment. Consequently, it is sufficient to pre-process FDR data using a linear Kalman Filter. The ASDE-X data, on the other hand, contains much more noise, since it is measured using onboard transponders as well as surface surveillance equipment. Therefore, much more elaborate filtering is required to make it usable for further analysis. This chapter describes the filter developed to pre-process ASDE-X data.

2.1 Introduction

2.1.1 Motivation

The availability of surface surveillance data allows us to visualize actual taxi routes of aircraft and to directly measure metrics such as total taxi distance, taxi time and time spent in the departure queue. These quantities form the basis for further studies such as the calculation of total fuel burn due to airport surface operations [2] or the

prediction of aircraft taxi-out times [3].

However, estimates produced using raw ASDE-X tracks are prone to error, because of inherent noise in the data. For example, noise in position data can lead to overestimation of taxi distance, noise in velocity data can lead to errors in detection of takeoff and landing, and noise in heading data can lead to false turn detection. In order to mitigate these effects, an unscented Kalman filter (UKF) [4, 5] in the multi-modal form was found to work very well. A bank of UKFs filters the raw data, with each filter representing a different taxi mode. The current taxi mode is detected by selecting the filter with the least (normalized) squared error, combined with a heuristic that offers resistance to rapid mode jumping.

The performance of the linear and extended versions of the Kalman filter [6] was also measured. The linear filter had insufficient noise suppression, while the extended Kalman filter was found to diverge often when applied to the current system. The unscented Kalman filter, on the other hand, was seen to be much more stable. Finally, the multi-modal filter formulation (MMF) was used because of its tracking accuracy and the relative ease of inferring taxi mode, when compared to a single filter. The multi-modal formulation has been previously used in areas such as computer vision [7], but it appears to have not been used for aircraft position tracking on the ground. The latter part of this chapter compares the performance of the MMF with a single-mode UKF.

2.1.2 Overview of ASDE-X data

The Airport Surface Detection Equipment, Model-X is primarily a safety tool designed to mitigate the risk of runway collisions [1]. It incorporates real-time tracking of aircraft on the surface to detect potential conflicts. There is potential, however, to use the data generated by it for surface operations analysis and aircraft behavior prediction. The data itself is generated by sensor fusion from three primary sources: (i) Surface movement radar, (ii) Multilateration using onboard transponders, and (iii) GPS-enabled Automatic Dependent Surveillance Broadcast (ADS-B). Reported parameters include each aircraft's position, velocity, altitude and heading. The up-

date rate is of the order of 1 second for each individual track. The coverage range is approximately 20 miles out from the airport.

All the ASDE-X data used here is from the Runway Status Lights (RWSL) system at Boston Logan International Airport (BOS). The results presented in this chapter are based on data from August to December 2010. As discussed above, the raw data contains a substantial amount of noise despite an upgrade installed in April 2010 to the system at Boston.

2.2 Formulation

As mentioned in the previous section, both the linear and the extended versions of the Kalman filter were tried without much success. The linear filter was unable to reduce noise to a satisfactory level without sacrificing accuracy, while the extended filter was prone to divergence. While 'truth' was not available in this study since the data was from actual operations, some idea of taxi path could be inferred from the raw trajectories superimposed over a layout of the taxiways in Google Earth®. Specifically, aircraft do not stray far from the centerlines marked on the taxiways/runways, allowing comparison of filter tracking behavior by visual inspection.

2.2.1 System Dynamics

The state vector to be estimated consists of aircraft position (X in meters east and Y in meters north), absolute velocity (V, m/s) and heading (θ, degrees):

$$\bar{x} = \begin{bmatrix} X & Y & V & \theta \end{bmatrix}' \tag{2.1}$$

The number of states is $n = 4$. To account for values of longitudinal acceleration and turn rate different from those in the system model, the velocity and heading states were assumed to have independent, zero mean, white Gaussian process noise with variance σ^2_{wV} and $\sigma^2_{w\theta}$ respectively. The assumption of independence meant that the

process noise covariance matrix Q was diagonal:

$$Q = \begin{bmatrix} \sigma_{wV}^2 & 0 \\ 0 & \sigma_{w\theta}^2 \end{bmatrix} \tag{2.2}$$

Since all four states are available in ASDE-X data, the measurement vector $\bar{y}$ had the same components as the state vector. It was assumed that noise variance involved in the measurement of X and Y positions was independent but had equal variance. The position, velocity and turn-rate noise variances were assumed to be equal to σ_{vxy}^2, σ_{vV}^2 and $\sigma_{v\theta}^2$ respectively. The measurement noise covariance matrix, R was therefore given by:

$$R = \begin{bmatrix} \sigma_{vxy}^2 & 0 & 0 & 0 \\ 0 & \sigma_{vxy}^2 & 0 & 0 \\ 0 & 0 & \sigma_{vV}^2 & 0 \\ 0 & 0 & 0 & \sigma_{v\theta}^2 \end{bmatrix} \tag{2.3}$$

Finally, the continuous nonlinear state dynamics were assumed to be:

$$\dot{\bar{x}} = \begin{bmatrix} \dot{X} \\ \dot{Y} \\ \dot{V} \\ \dot{\theta} \end{bmatrix} = \begin{bmatrix} V \sin\theta \\ V \cos\theta \\ a \\ \omega \end{bmatrix} + B_w \bar{w} \tag{2.4}$$

Here, a is the longitudinal acceleration and ω is the turn rate, both of which are assigned different constant values in the system model for each mode. Since a heading of zero degrees is due north, the sine component of velocity affects X position while the cosine component affects Y position. A full list of taxi modes is given in Table 2.1. For the single-mode UKF used for comparison purposes, the assumed values were $a = \omega = 0$. The additive noise term in (2.4) is the product of the the matrix B_w and the process noise $\bar{w}$. The noise vector $\bar{w} = [w_V \quad w_\theta]'$ contains noise in acceleration and turn rate, and is assumed to vary like $\mathcal{N}(\mathbf{0}, Q)$. The matrix B_w ensures that $\bar{w}$

affects only velocity and turn rate, and is given by:

$$B_w = \begin{bmatrix} 0 & 0 \\ 0 & 0 \\ 1 & 0 \\ 0 & 1 \end{bmatrix} \tag{2.5}$$

The measurement vector is equal to the state vector with an additive noise term:

$$\bar{y} = \bar{x} + \bar{v} \tag{2.6}$$

Here $\bar{v} = [v_X \quad v_Y \quad v_V \quad v_\theta]'$ is the measurement noise vector, assumed to be independent of process noise, white, Gaussian and to vary like $\mathcal{N}(\mathbf{0}, R)$. The diagonal covariance matrix R ensures that the elements of measurement noise are independent of each other.

Mode Number	Description	Longitudinal Acceleration a (m/s^2)	Turn Rate ω (deg/s)
1	Default	0	0
2	Moderate Acceleration	1	0
3	Moderate Deceleration	-1	0
4	Constant Speed Turn Right	0	10
5	Constant Speed Turn Left	0	-10
6	Accelerating Turn Right	3	10
7	Accelerating Turn Left	3	-10
8	Decelerating Turn Right	-3	10
9	Decelerating Turn Left	-3	-10
10	High Acceleration	3	0
11	High Deceleration	-3	0

Table 2.1: List of taxi modes

2.2.2 Form of filter

Definition of Constants

The UKF formulation used for each mode was based on the method proposed by Wan and van der Merwe [4]. According to this method, a state vector of length n results in $(2n+1)$ sigma points. Some additional required constants are defined below. Note that in this case, the number of states is $n = 4$.

$$\kappa = 3 - n \tag{2.7a}$$

$$\alpha = 0.5 \tag{2.7b}$$

$$\lambda = \alpha^2(n + \kappa) - n \tag{2.7c}$$

$$\beta = 2 \tag{2.7d}$$

Based on these constants, the weights used for generation of the $(2n+1)$ sigma points from the sigma point generator matrix are defined.

$$w_{c,i} = \frac{1}{2(n+\lambda)} \qquad \text{for} \quad i = 1, 2, ..., 2n \tag{2.8a}$$

$$w_{c,2n+1} = \frac{\lambda}{n+\lambda} + 1 - \alpha^2 + \beta \tag{2.8b}$$

$$w_{m,j} = \frac{1}{2(n+\lambda)} \qquad \text{for} \quad j = 1, 2, ..., 2n \tag{2.8c}$$

$$w_{m,2n+1} = \frac{\lambda}{n+\lambda} \tag{2.8d}$$

Finally, the discrete equivalent process noise covariance matrix, Q_d, is based on the approximation (2.9), with T_s the time difference between two successive measurements. Note that Q_d is of size 4×4.

$$Q_d \approx B_w Q B_w^T T_s \tag{2.9}$$

Filter Algorithm

Let us define the quantity $z_k^{(i)+}$ to be the value of the generic quantity z after the measurement update at time step k, for the i^{th} sigma point where $i = 1, 2, ..., 2n + 1$.

Similarly, $z_{k+1}^{(i)-}$ is the quantity z propagated to time step $k+1$ but prior to the measurement update at time step $k+1$. Let $\hat{\bar{x}}$ denote the estimated state vector, $\bar{x}^{(i)}$ denote the i^{th} sigma point, $\bar{y}$ denote actual measurements, $\hat{\bar{y}}$ be the expected measurement vector and P be the sigma point generator matrix, viz. the uncertainty matrix from which sigma points are generated. The filter algorithm [4] is given below. Since all the states are available for measurement, algorithm initialization is done using $\hat{\bar{x}}_0^+ = \bar{y}_0$ (first detection of current aircraft) and $P_0^+ = R$.

1. Generation of sigma points at time step k, with the i^{th} sigma point generated using the transpose of the i^{th} row belonging to the matrix square root of $(n+\lambda)P_k^+$:

$$\begin{aligned}
\bar{x}_k^{(i)+} &= \hat{\bar{x}}_k^+ + [\{\sqrt{(n+\lambda)P_k^+}\}^{(i)}]^T \quad \text{for} \quad i = 1, 2, ..., n \\
&= \hat{\bar{x}}_k^+ - [\{\sqrt{(n+\lambda)P_k^+}\}^{(i)}]^T \quad \text{for} \quad i = (n+1), (n+2), ..., 2n \\
&= \hat{\bar{x}}_k^+ \quad \text{for} \quad i = 2n+1
\end{aligned}$$

2. Propagation of belief to the next time step, with a_f and ω_f being the acceleration and turn rate values assumed in the system model for filter f. The propagation equations are based on simple kinematics.

$$\bar{x}_{k+1}^{(i)-} = \bar{x}_k^{(i)+} + \begin{bmatrix} (V_k^{(i)+} T_s + \frac{1}{2} a_f T_s^2) \sin(\frac{\pi}{180} \theta_k^{(i)+}) \\ (V_k^{(i)+} T_s + \frac{1}{2} a_f T_s^2) \cos(\frac{\pi}{180} \theta_k^{(i)+}) \\ a_f T_s \\ \omega_f T_s \end{bmatrix}$$

3. Calculation of expected state vector at step $k+1$ from the propagated sigma points:

$$\hat{\bar{x}}_{k+1}^- = \sum_{i=1}^{2n+1} w_{m,i} \bar{x}_{k+1}^{(i)-}$$

4. Estimation of the uncertainty covariance matrix:

$$P_{k+1}^{-} = Q_d + \sum_{i=1}^{2n+1} w_{c,i}(\bar{x}_{k+1}^{(i)-} - \hat{\bar{x}}_{k+1}^{-})(\bar{x}_{k+1}^{(i)-} - \hat{\bar{x}}_{k+1}^{-})^T$$

5. Recalculation of sigma points $\bar{x}_{k+1}^{(i)-}$ using the same equations as in step 1, but with P_{k+1}^{-} as the generating matrix. The measurement sigma points, $\bar{y}_{k+1}^{(i)}$, are equal to $\bar{x}_{k+1}^{(i)-}$ since full state measurement is available.

6. Calculation of expected measurement vector at step $k+1$:

$$\hat{\bar{y}}_{k+1} = \sum_{i=1}^{2n+1} w_{m,i}\bar{y}_{k+1}^{(i)}$$

7. Calculation of the Kalman filter gain at time step $k+1$, L_{k+1}:

$$P_{yy} = R + \sum_{i=1}^{2n+1} w_{c,i}(\bar{y}_{k+1}^{(i)} - \hat{\bar{y}}_{k+1})(\bar{y}_{k+1}^{(i)} - \hat{\bar{y}}_{k+1})^T$$

$$P_{xy} = \sum_{i=1}^{2n+1} w_{c,i}(\bar{x}_{k+1}^{(i)-} - \hat{\bar{x}}_{k+1}^{-})(\bar{y}_{k+1}^{(i)} - \hat{\bar{y}}_{k+1})^T$$

$$L_{k+1} = P_{xy}P_{yy}^{-1}$$

8. Belief update using actual measurement at time step $k+1$, $\bar{y}_{k+1}$:

$$\hat{\bar{x}}_{k+1}^{+} = \hat{\bar{x}}_{k+1}^{-} + L \cdot (\bar{y}_{k+1} - \hat{\bar{y}}_{k+1})$$

$$P_{k+1}^{+} = P_{k+1}^{-} - LP_{yy}L^T$$

This algorithm is run simultaneously on all filters in the bank. The expected measurement from each filter is compared to the actual measurement vector. Based on this comparison, the current taxi mode is set, and the state estimate from the corresponding filter becomes the new state estimate for the entire bank. The algorithm then repeats, starting from step 1.

Selection of Taxi Mode

The selection of taxi mode is based upon a *Quality Index* (QI) that is essentially the negative of the second-order norm of the residual for each filter, normalized by the measurement noise covariance.

$$\text{QI} = -(\bar{y}_{k+1} - \hat{\bar{y}}_{k+1})^T R^{-1} (\bar{y}_{k+1} - \hat{\bar{y}}_{k+1}) \tag{2.10}$$

The filter selection algorithm tracks the Quality Index for each filter, for the latest three time steps. The particular filter selected is the one that has the *maximum* QI, among all f filters, for the *most* times in these three time steps. If three different filters have one instance each of maximum QI in the last three time steps, the incumbent filter continues to be selected. The algorithm is initiated at the start of each flight track with the 'straight, constant velocity' mode active.

A Gaussian likelihood estimate, based on the measurement error of each filter, and the uncertainty as derived from the matrix P, was initially tested as the criterion for mode selection. However, it was found that the measurement noise can cause the error to be occasionally so large that all likelihood values drop to machine zero. In addition, the evaluation of Gaussian likelihood requires a call to a separate subroutine in the code, and is computationally expensive. Therefore, the second-order norm was chosen as a measure of likelihood. The additional heuristic of choosing the best filter over the last three time steps helps avoid frequent mode jumping caused by erratic measurement errors.

2.3 Results

2.3.1 Multi-Modal Filter Output

A comparison of the output from the multi-modal filter with raw data is shown in Figure 2-1, while Figure 2-2 shows sample output for a departure and an arrival. Figure 2-1 is from a portion of taxiway close to the threshold of Runway 33L at Boston Logan. The white line in the upper plot traces the raw data, while the multi-colored segmented line in the lower plot is the filter output. It can be seen that most of the noise in the raw data has been filtered out by the MMF. At the same time, an idea about tracking performance of the filter can be obtained by observing that filtered output in all the figures is fairly close to the taxiway markings on the surface. Note that the colors in the filter output indicate the taxi mode as detected by the filter. Table 2.2 relates the colors to the taxi modes from Table 2.1.

Taxi Mode	Mode Numbers	Color
Raw data	-	White
Straight, constant speed	1, 2, 3	Dark Blue
Decelerating straight / turn	8, 9, 11	Red
Accelerating straight / turn	6, 7, 10	Green
Turn, constant speed	4, 5	Light Blue

Table 2.2: Color coding for Figures 2-1 and 2-2

Figure 2-3 shows results from the taxi mode detection algorithm for a specific flight. It can be seen that the code correctly detects a constant speed turn (starting at 756 seconds on the X axis) followed by takeoff, which is a period of sustained high acceleration. Note that the fourth plot in the figure shows *relative* Quality Index values for each mode, i.e., the difference between the Quality Index of each filter and the instantaneous Quality Index of the default mode having $[a, \omega] = [0, 0]$.

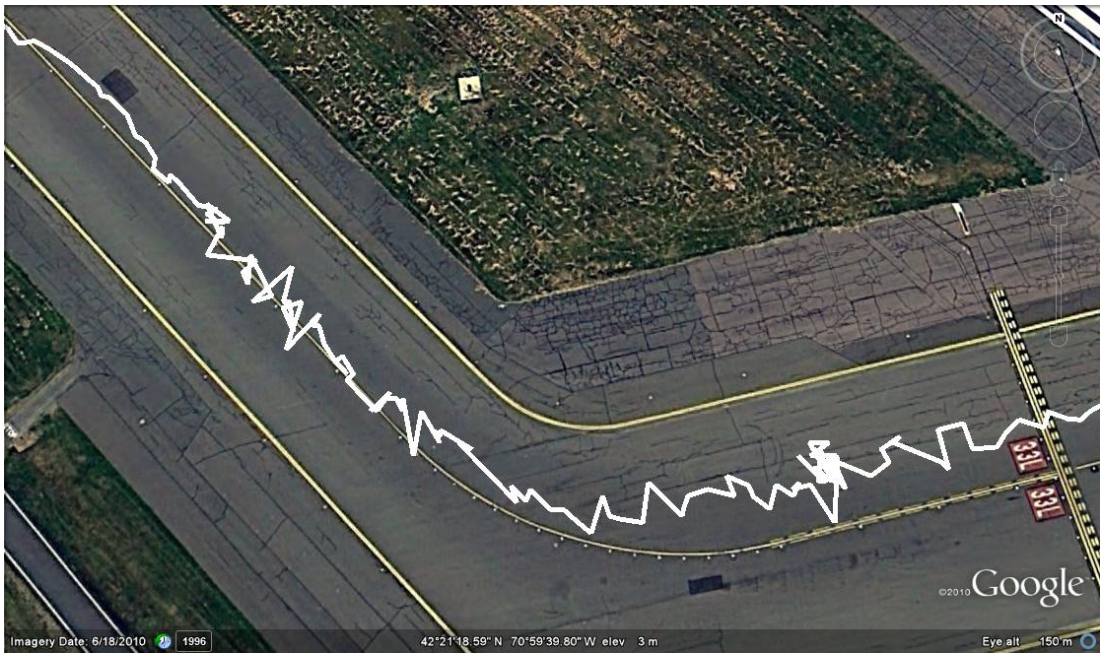

(a) Raw Data

(b) MMF Output

Figure 2-1: Sample output from Multi-modal Filter. Both pictures correspond to the area enclosed by the orange rectangle in the inset image.

(a) Arriving flight: Landing on the runway is seen on the right, with strong braking marked in red. The flight then leaves the runway and taxis towards its gate beyond the top edge of the picture. Portions where a turn was detected are marked in light blue.

(b) Departing flight: Departure is on Runway 4R, with acceleration phase indicated in green.

Figure 2-2: Sample MMF output

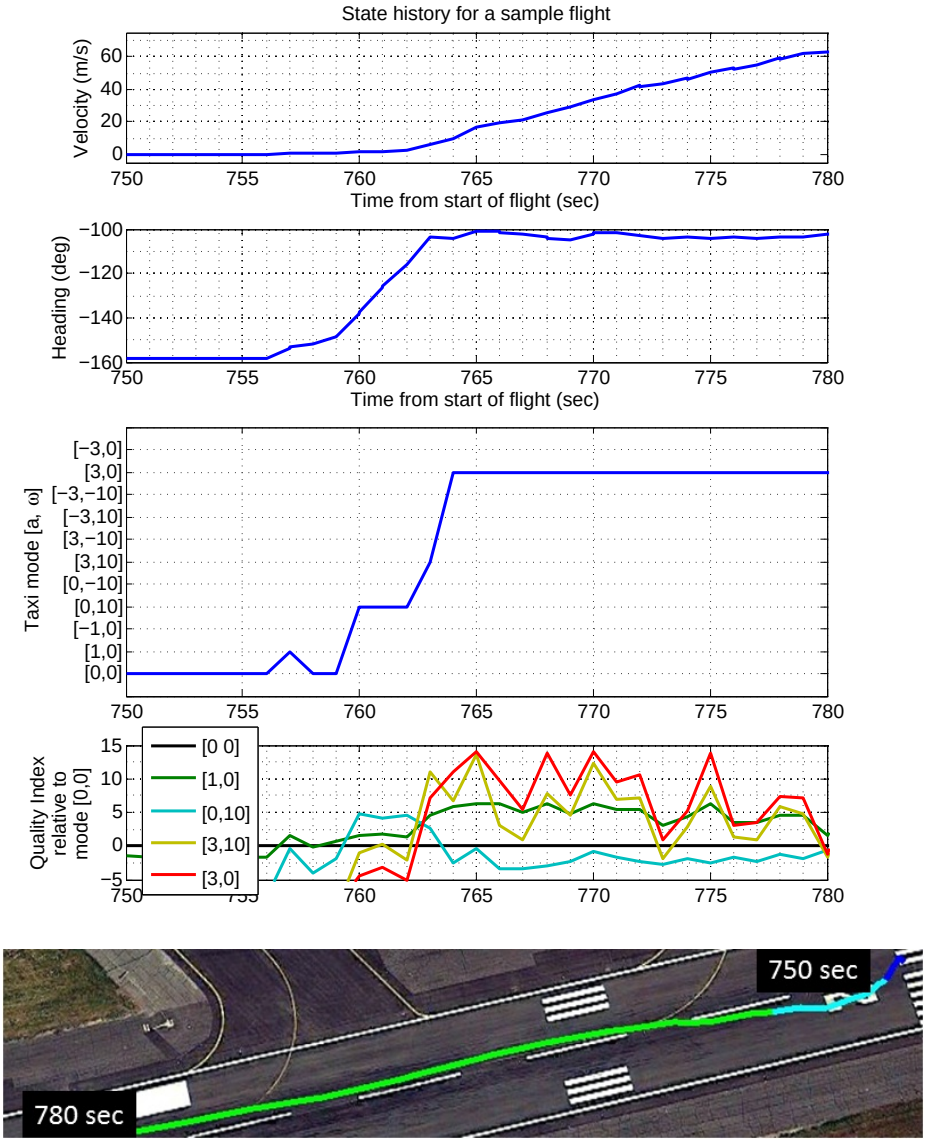

Figure 2-3: Taxi mode detection for a sample flight. The first two plots show velocity and heading for the aircraft trajectory shown in the bottom plot. The third plot shows the output of the mode detection algorithm, with acceleration and turn-rate values of each mode marked on the Y axis. The fourth plot shows the quality index of the best five modes in this time period, *relative* to the baseline mode $[a, \omega] = [0, 0]$.

Figures 2-4 and 2-5 are typical examples of the noise in raw data. In Figure 2-4, considerable jitter is seen in the measured Y position, most of which is removed by the filter. There is some noise in the X position as well, but not much in the velocity and heading fields. In Figure 2-5, there is noise in velocity and heading but not in position. Note that each of the four fields is independently measured by the

ASDE-X system, and therefore, measured velocity is not simply the derivative of position. Finally, Figure 2-6 shows autocorrelation plots of the estimation residuals for a single flight. For each measurement variable, it shows the correlation coefficient of the residual (error) at one time step with all other residuals in the rest of the flight track. The low value of correlation except where the difference in index goes to zero (correlation with itself) indicates that the residuals are a white sequence [8, 9], and therefore the filter is working efficiently.

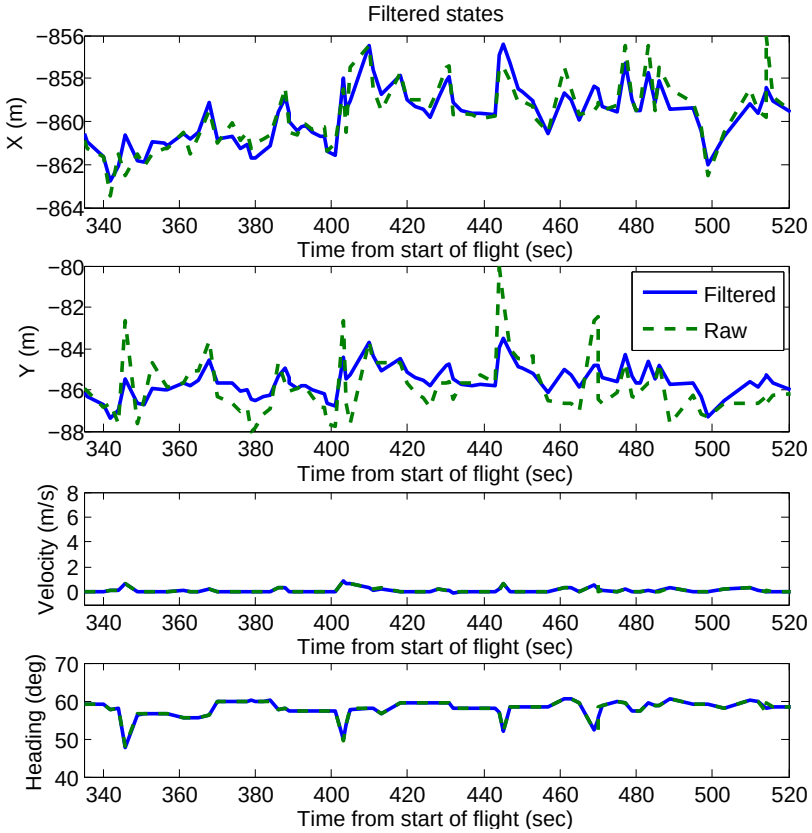

Figure 2-4: Comparison of raw data and filtered output for a sample flight with noise seen in position measurement

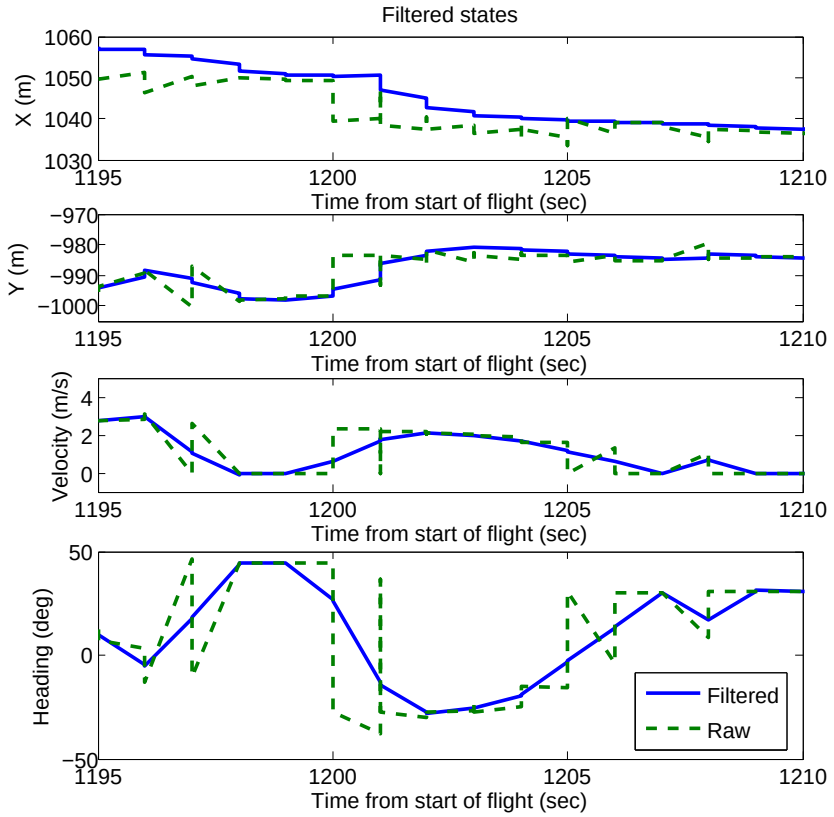

Figure 2-5: Comparison of raw data and filtered output for a sample flight with noise seen in heading and velocity measurement

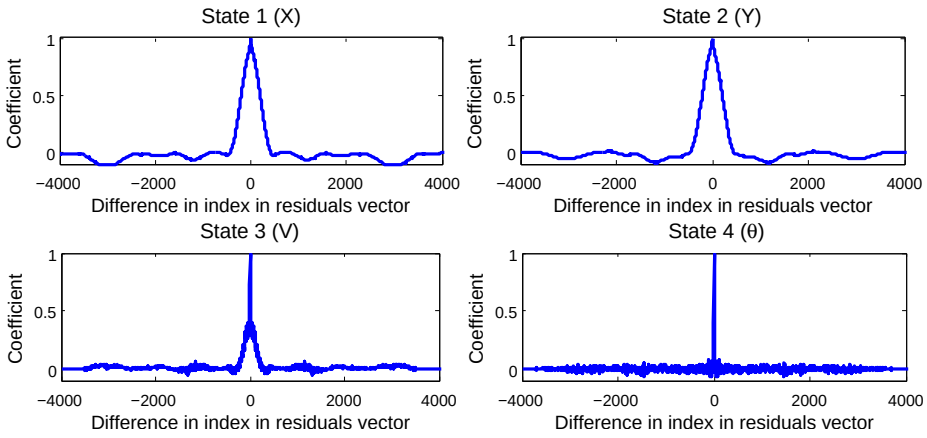

Figure 2-6: Autocorrelation of residuals for a single sample flight

2.3.2 Comparison with single-mode UKF and Raw data

In terms of output quality, the single-mode UKF formulation ends up being inferior to the multi-modal form. This is primarily due to the fact that the process model in the single-mode UKF only accounts for straight, constant speed taxi. If noise suppression comparable to the MMF is desired, the assumed measurement noise covariance needs to be so high that the filter fails to track quick changes in velocity and heading. For example, Figure 2-7 shows the filter output belatedly tracking a turning aircraft, thus producing an estimate of position which is unrealistically close to the edge of the taxiway.

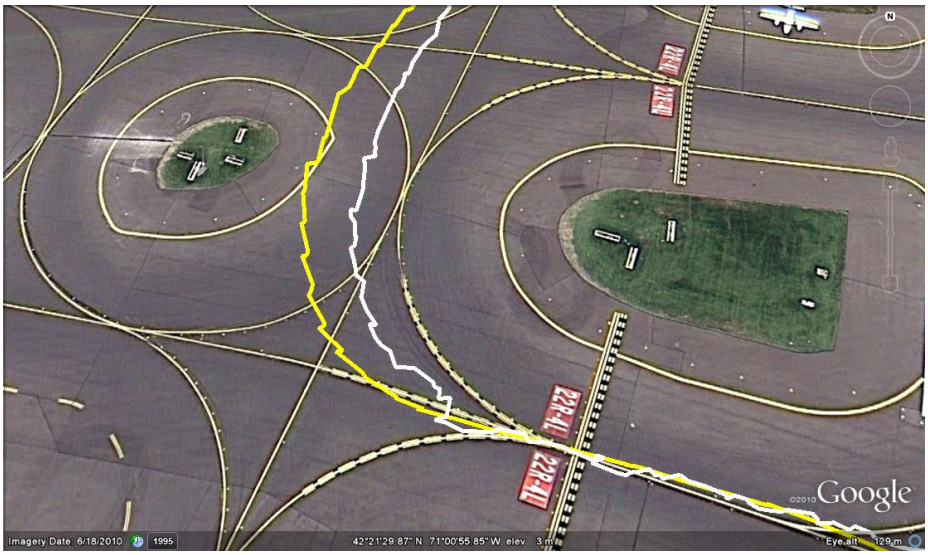

Figure 2-7: Sample result from single-mode UKF: Raw data in white, UKF output in yellow

Figure 2-8 gives an idea of the relative tracking behavior of the filters discussed so far. It shows the mean ratio of the taxi distance measured using three different methods for a total of 20 flights, to the taxi distance measured visually by a straight-line approximation of the taxi path. The three ways in addition to the visual measurement, by which taxi distances have been calculated are (i) using the MMF, (ii) using the single-mode UKF, and (iii) from raw data. The normalization of taxi distance in this manner accounts for different taxi paths used by different flights. As seen in the figure, the mean distance measured by the MMF is closest to the straight-line

method. Note that the MMF output is likely to be closer to actual taxi distance than the straight-line approximation since aircraft do not stick strictly to taxiway centerlines. It is clear from the figure, though, that taxi distance calculated using raw data would hold very little value for further analysis, because of its large taxi distance estimates. Further, the large variance precludes the use of constant-factor scaling to increase the accuracy of the raw estimates.

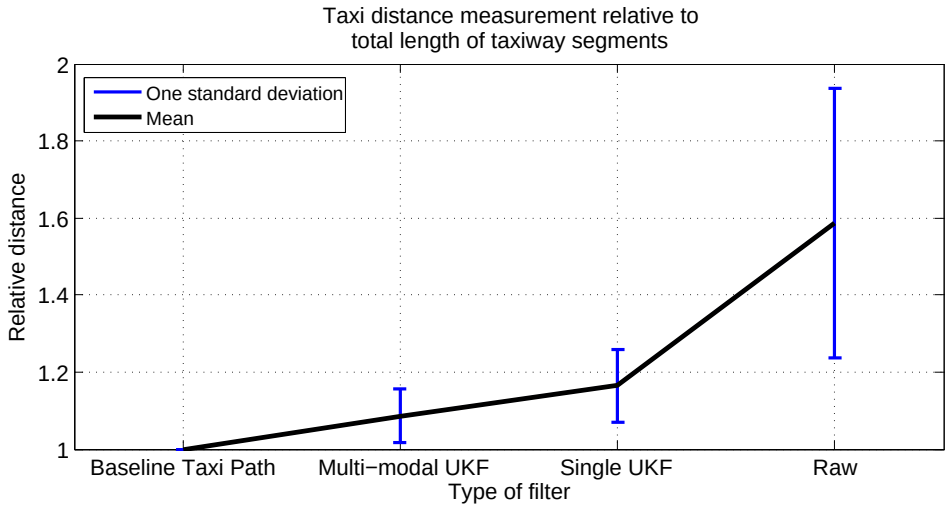

Figure 2-8: Comparison of taxi-out distance ratios

2.4 Summary

In this chapter, it was showed that the raw data contained a significant amount of noise, precluding its direct application to further analysis such as taxi distance calculations. The MMF was shown to successfully mitigate the effect of noise, while maintaining tracking performance. Tradeoffs involved with the use of a single-mode UKF instead of the MMF were considered. It was found that the MMF had better tracking properties than the UKF, making it the filter of choice for applications requiring accurate estimates of aircraft position and taxi mode. In subsequent chapters, all the ASDE-X data has been pre-processed using either the single-mode UKF or the MMF, depending on the accuracy required and the amount of data to be processed.

Chapter 3

Characterization of Airport Surface Operations

3.1 Introduction

Airports form the critical nodes of the air transportation network, and their performance is a key driver of the capacity of the system as a whole [10]. With several major airports operating close to their capacity, the smooth and efficient operation of airports is essential for the efficient functioning of the air transportation system. Studies of airport operations have traditionally focused on airline operations and on the aggregate estimation of airport capacity envelopes [11, 12, 13, 14]. Most of this research is based on data from a combination of the Aviation System Performance Metrics (ASPM) [15] and the Airline Service Quality Performance (ASQP) systems. These databases, when in individual aircraft format, provide the times at which flights pushback from their gates, their takeoff and landing times, and the gate-in times, as reported by the airlines. ASPM also provides airport-level aggregate data, which enumerates the total number of arrivals and departures in 15-minute increments. Such data can be used to develop queuing models of airport operations [16, 17] or empirically estimate airport capacity envelopes [13]. However, this level of detail is typically insufficient to investigate other factors that affect surface operations, such as interactions between taxiing aircraft, runway occupancy times, etc. As outlined in the

previous chapter, ASDE-X data does provide the level of detail that allows analysis of aircraft interaction in a disaggregate sense. This chapter describes the ways in which ASDE-X data can be leveraged to characterize airport surface operations, and proposes methods to track airport operational performance.

The filtering algorithm described in Chapter 2 processes the ASDE-X flight tracks, one full day at a time. These filtered quantities are then used to tag each valid flight track with a departure/arrival time and runway. By tracking each aircraft from pushback to wheels-off, various airport states such as the active runway configuration, location and size of the departure queue, and departure/arrival counts are measured. In addition, airport-level performance metrics such as average taxi-out times, runway usage and inter-departure spacing statistics are also tracked. The definitions of these metrics and the algorithms proposed for measuring them are described in subsequent sections of this chapter.

3.2 Airport Operational Characteristics

3.2.1 Departure Queue Characteristics

Visualization of the filtered ASDE-X data gives insights into the dynamics of airport operations. For example, locations on the surface where aircraft typically queue up for departure can be determined. These locations depend on the runway configuration and operational procedures. For example, Figure 3-1 (left) shows the layout of BOS. Figure 3-1 (right) shows the departure queues formed on a day in September 2010 in the 22L | 22R configuration, i.e., when runway 22L (on the east side) was being used for arrivals and 22R (on the west side) was being used for departures.

There is a primary departure queue at the runway threshold, and a secondary one before it. The secondary queue is composed of aircraft waiting to cross the departure runway on their way to the primary queue. During the months of August and September 2010, there was taxiway construction at BOS, which closed the taxiway area denoted by white in the the figure.

Figure 3-1: (Left) Layout of Boston Logan International Airport. (Right) Visualization of airport operations. Aircraft in green are departures and the ones in red are arrivals. A previously arrived aircraft can be seen at the bottom of the picture, waiting to cross the departure runway on the way to its gate.

Observation of operations over several days of data provided an insight into typical queue formation areas. These areas were then designated in the analysis codes for automatic tracking of departure queues and calculation of statistics such as time spent by individual aircraft in the queue and the variation of queue length over each day. Figure 3-2 shows the variation of mean time spent in the primary departure queue,

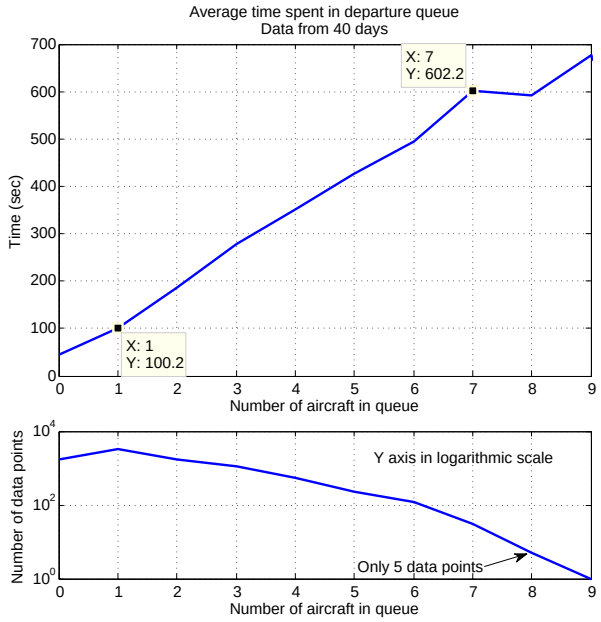

Figure 3-2: Variation of mean time spent in the departure queue with departure queue length at the time of a flight joining it

with the queue length. It is based on 40 days of data from all runway configurations. We define queue length as the number of aircraft in the primary departure queue as seen by a new aircraft just joining it. It can be seen that on average, each additional aircraft in queue entails a penalty of 83 seconds for all the aircraft behind it. This value seems to be reasonable when compared to the standard departure separations described in Section 3.3.3.

3.2.2 Departure Throughput Characteristics

Departure queue characterization offers an insight into surface operations from an aircraft's perspective. Airport-level operational performance was tracked using the variation of departure throughput (defined as the number of takeoffs in a 15-minute interval) with the number of active departing aircraft on the surface. Aircraft were defined to be active from the time of first transponder capture (first detection with ASDE-X) to wheels-off time. Previous studies [17, 18] have shown, using ASPM data, that the increment in departure throughput decreases with the addition of aircraft to the surface, finally leading to saturation. This is corroborated by the results produced using ASDE-X data. Figure 3-3 shows the departure throughput curve for a specific configuration at Boston. Note that only jet aircraft are counted in this analysis. This is because propeller-driven aircraft are fanned out via separate departure fixes at Boston, thus not affecting the jet departure process. The throughput curves for other configurations are similar in nature to Figure 3-3, differing only in the point of saturation and maximum throughput. These differences can be attributed to configuration-specific procedures, such as closely spaced departures on intersecting runways.

3.3 Operational Performance Metrics

Building on the results described in the previous section, it is possible to develop metrics to measure an airport's operational performance. The motivation is not to scrutinize controller performance, but to look for systematic inefficiencies and to iden-

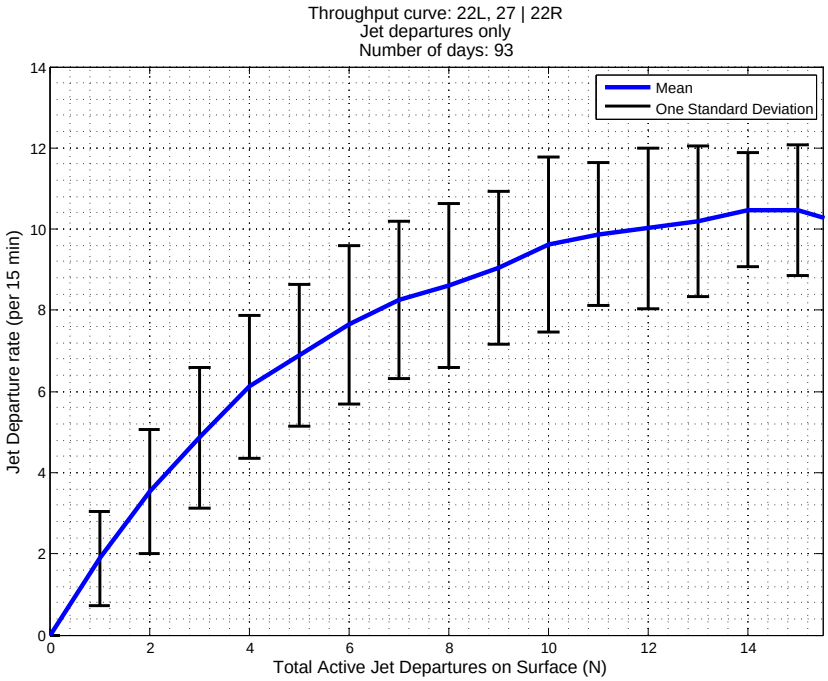

Figure 3-3: Departure throughput saturation: 22L, 27 | 22R configuration.

tify opportunities for improvement. The basic concepts used to define these metrics are generalizable to any airport. However, each airport has local rules, regulations and procedures that must be considered in order to be consistent across different configurations and time periods. For example, there are subtle variations in the strategies used by different airports to accommodate both arrivals and departures on the same runway or on intersecting runways. At Boston, arrivals have to cross the departure runway in the 22L, 27 | 22R configuration. On the other hand, in the 27 | 33L configuration, it is the departures that have to cross the arrival runway. Arrivals at Boston are controlled by the Boston Center, and consequently, they receive priority over departures. Their sequence and separation is not controlled by the tower. The following discussion presents the performance metrics, developed in consulation with Boston ATC, that account for as many of these complexities as possible while keeping the computational effort at a reasonable level.

3.3.1 Average Taxi-out Times

The most natural performance measure from the point of view of passengers is the average taxi-out time for departures. This is an important quantity that affects not only flight delays but also taxi-out fuel consumption. In general, taxi-out times are highest in the peak congestion periods. At Boston, these are the morning departure push at around 0600 hours local, and the evening push between 1900 and 2000 hours local time. Figure 3-4 shows the variation of average taxi-out times on a sample day. The averages are calculated over 15 minute intervals for the entire day. Each bar in the upper plot represents the average taxi-out time experienced by the aircraft pushing back in that 15 minute interval. The number of pushbacks in the corresponding interval are shown in the lower plot. The peaks in both pushbacks and taxi-out times around 0600 and 2000 can be seen clearly. Note that in the calculation of this metric, the time spent by aircraft absorbing departure holds, has been subtracted. These aircraft usually have specified departure times known as Expected Departure Clearance Times (EDCTs), decided by constraints elsewhere in the National Airspace System (NAS). While it is desirable to have aircraft absorb these delays at the gate, it is not always possible because of conflicts with arrivals that are scheduled to dock at the same gate. Figure 3-5 shows a similar plot as Figure 3-4, but with flights with EDCTs included in the data. A comparison of the two plots illustrates the effect of excluding these flights.

3.3.2 Runway Utilization

The most capacity-constrained element in departure operations is the runway [19]. Therefore, it is important to ensure that an airport's runway system is used as efficiently as possible. To look at the current usage characteristics of runways at Boston, a metric called Runway Utilization was defined. The utilization is expressed as a percentage, calculated for every 15 minute interval. It is given by the fraction of time in the 15 minute interval for which a particular runway is being used for active operations. The types of active operations considered were:

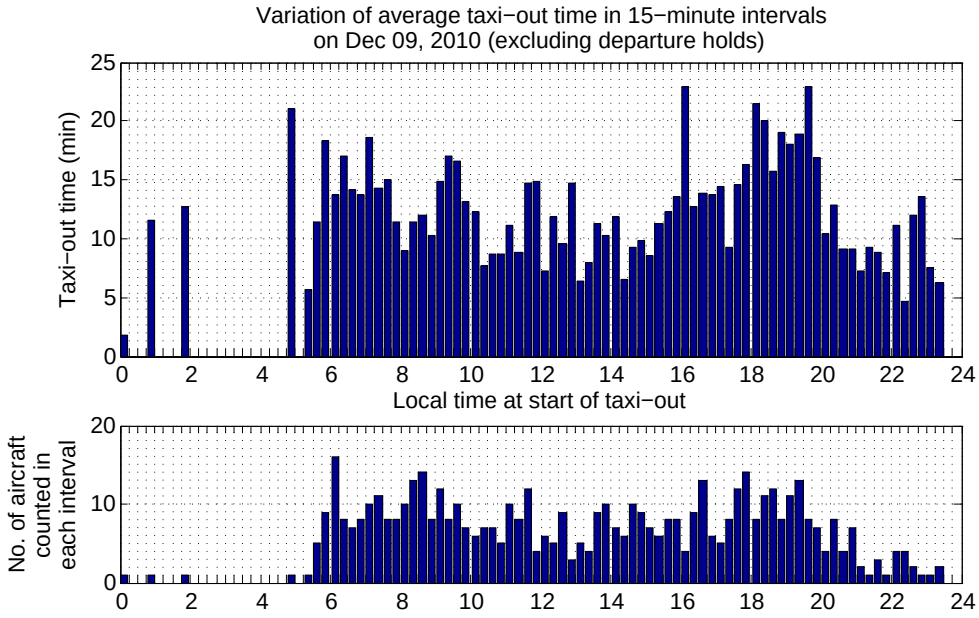

Figure 3-4: Variation of average taxi-out times on Dec 09, 2010. Flights with long holds due to EDCTs have been removed from the calculation of average taxi-out times.

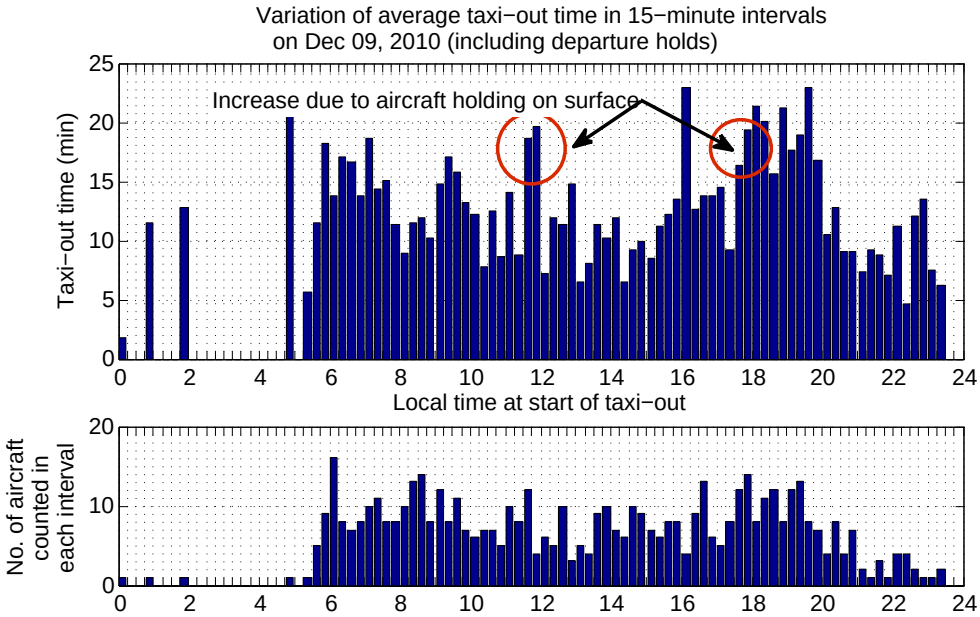

Figure 3-5: Variation of average taxi-out times on Dec 09, 2010, including flights with EDCTs.

1. Departure roll: Counted from the start of takeoff roll to wheels off

2. Departure hold: A departing aircraft holding stationary on the runway, waiting for takeoff clearance

3. Approach: Counted from the time an aircraft is on short final (within 2.5 nm of runway threshold) to the time of touchdown

4. Arrival: Counted from the moment of touchdown to the time when the aircraft leaves the runway

5. Crossings/Taxi: When aircraft are either crossing an active runway, or taxiing on an inactive runway

Each of these operating modes was detected using the filtered states from ASDE-X tracks for each aircraft. The 'approach' phase was included in the runway utilization because no other operations can be carried out on the arrival runway, or a crossing departure runway, when an aircraft is on short final. Even though, technically, the aircraft is not on the runway, ignoring this operational constraint would give erroneously low utilization figures.

Figures 3-6 to 3-8 show the utilization plots for a sample day, for three different runways. The topmost plot in each figure shows the breakup of utilization for the runway over the course of the day. The plot in the middle shows operational counts in each 15 minute interval, for both ends of the runway. Finally, the lowermost plot shows the variation of queue length over the day. It should be noted that the queue length is calculated for every second, while the top two plots are aggregate figures over the 15 minute interval. Details such as configuration changes can be seen immediately from the utilization plots. For example, we can see from Figures 3-7 and 3-8 that departure operations shifted from runway 22R to runway 33L at 1000 hours.

Ideally, it would be desirable to have the utilization figures be 100% for the active runways in times of peak demand. The sample figures show that while this figure is achieved for much of the peak period, it is difficult to sustain. Disruptions may be caused by off-nominal events such as runway closures due to foreign objects, arrivals

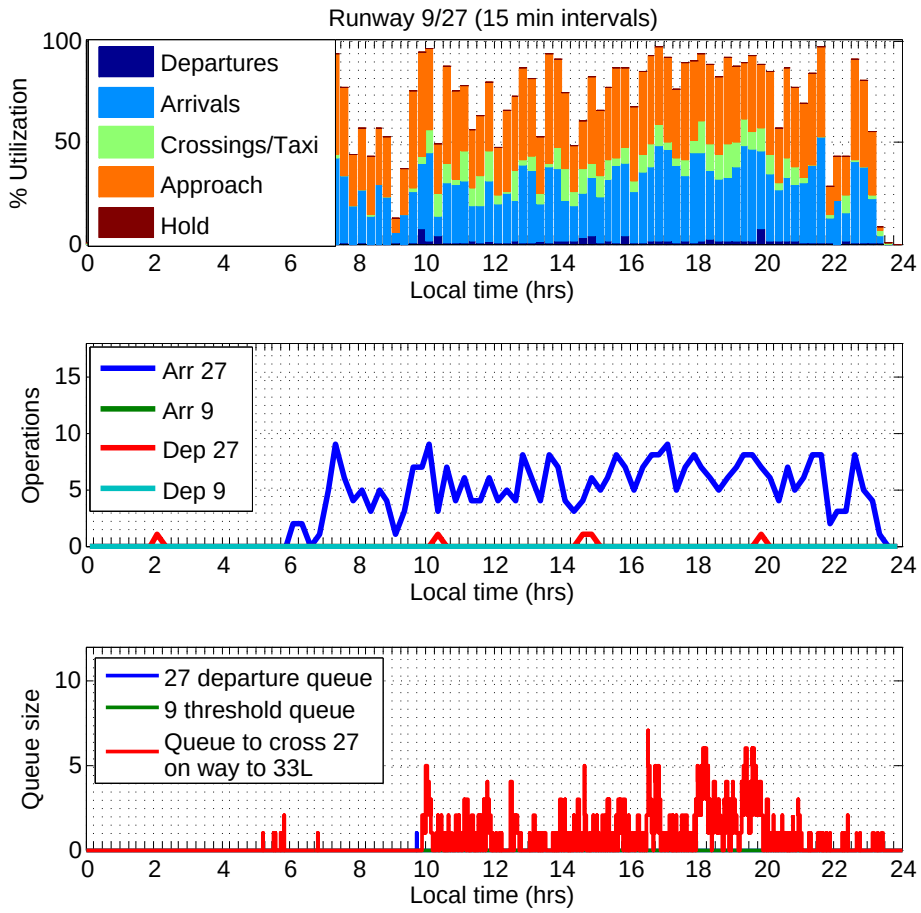

Figure 3-6: Utilization of Runway 9/27 on Dec 09, 2010. Runway 27 was used for arrivals for the entire day. An occasional departure can be seen in the second plot, accompanied by a dip in the number of arrivals and the utilization for the time period. In the bottom plot, queue formation can be seen, composed of aircraft waiting to cross the runway for departure on 33L.

requesting a departure runway for landing, or gaps in the arrival sequence. It should be noted that the utilization for the departure runway is always higher than that for the arrival runway. This is because the departures can be packed close together, with the next aircraft in queue holding on the runway while the previous aircraft starts its climb-out. On the other hand, tightly packed arrivals increase the risk of frequent go-arounds caused by aircraft not vacating the runway quickly enough to allow the next arrival to land. Therefore, the arrival stream usually has a buffer over and above the minimum spacing dictated by standard procedures.

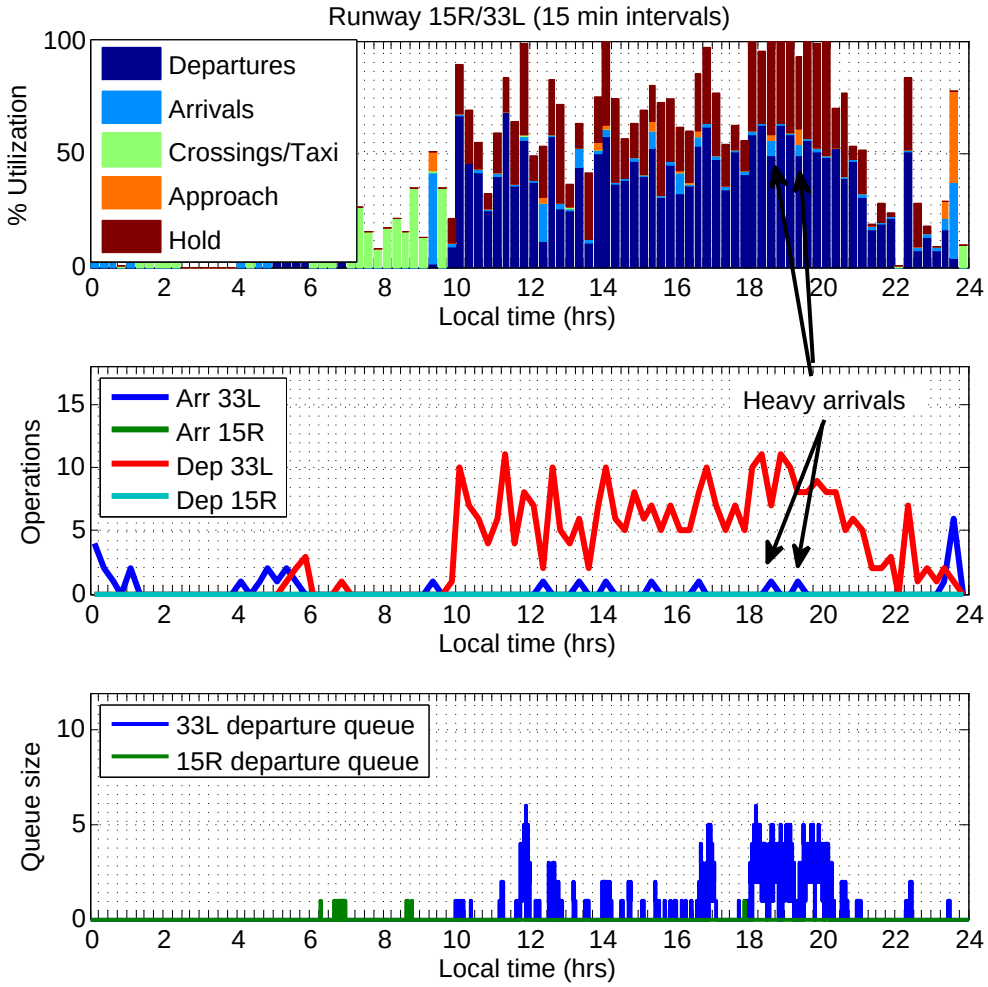

Figure 3-7: Utilization of Runway 15R/33L on Dec 09, 2010. Runway 33L was inactive until 1000 hours, after which it was used for departures. Occasional arrivals seen in the second plot are heavy aircraft requesting this runway for landing due to its greater length. Arrivals in the peak period between 1800 and 2000 cause a noticeable dip in the utilization.

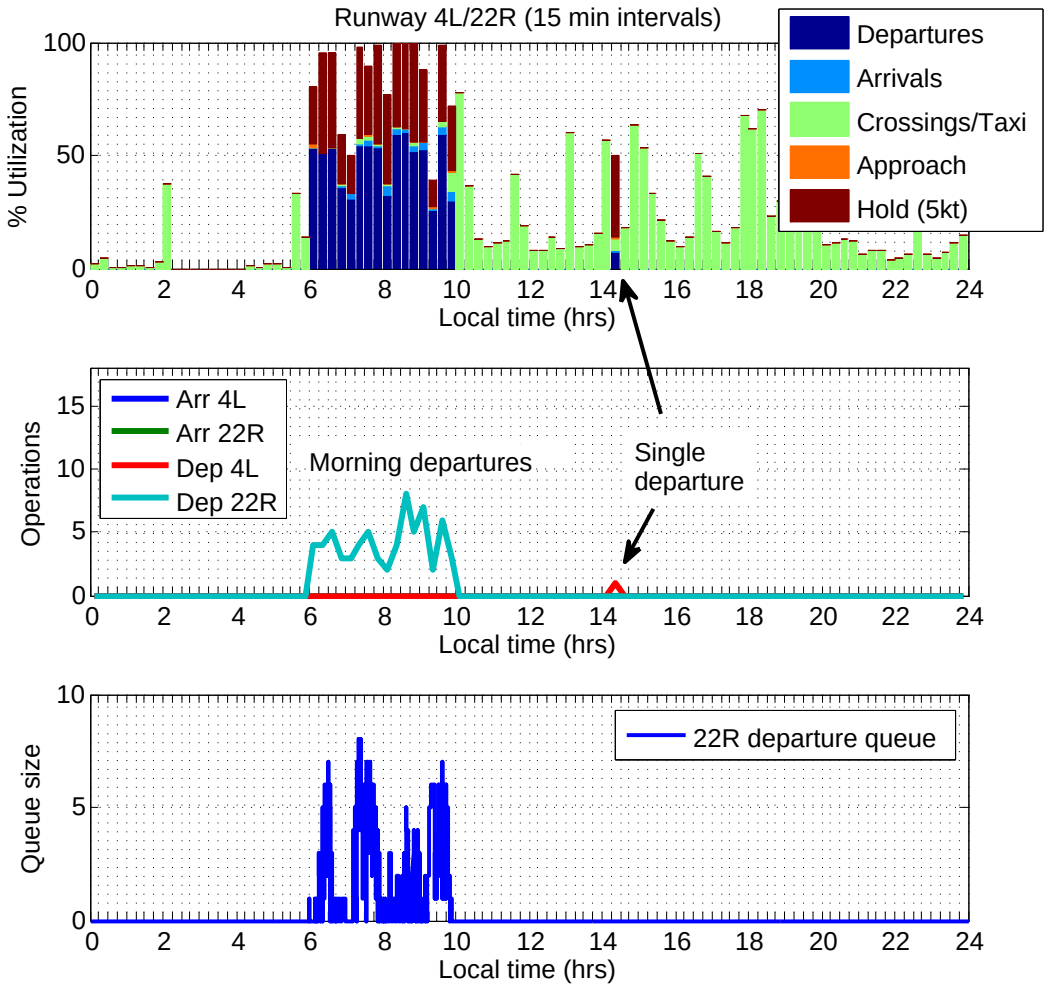

Figure 3-8: Utilization of Runway 4L/22R on Dec 09, 2010. Runway 22R was used for departures during the morning peak period. Note the longer queue lengths seen here, compared to those for runway 33L. This is because the morning demand is concentrated into two banks at 0600 and 0745 hours.

3.3.3 Departure Spacing Efficiency

As noted earlier, departures can be spaced more tightly compared to arrivals. However, the minimum departure spacing is still governed by a set of standards, customized to each airport depending on the runway and airspace layout. It is generally recommended to maintain a minimum spacing of 120 seconds for a departure following a heavy aircraft [20]. At Boston, the target separations, based on a combination of regulatory requirements and historical performance, are as given in Table 3.1.

	P	S	L	757	H
P	40	40	40	40	40
S	40	65	65	65	65
L	40	65	65	65	65
757	110	110	110	110	110
H	120	120	120	120	120

Table 3.1: Target departure separations. The columns correspond to the weight class of the trailing aircraft, while the rows correspond to the weight class of the leading aircraft. All figures are in seconds.

To compare the actual inter-departure separation with these target values, a metric called the Departure Spacing Efficiency was defined. As with runway utilization, this metric is calculated for each 15 minute interval. However, the Departure Spacing Efficiency is not runway-specific, but addresses departure operations at the airport as a whole. To calculate it, the difference between the wheels-up times of each pair of consecutive departures is compared to the target level of separation for that pair, based on the aircraft classes of the leading and trailing aircraft. Each additional second more than the target level is counted as a second *lost*. Time is counted as 'lost' only if there are other aircraft in queue, waiting for departure. This ensures that the efficiency figure does not fall simply because of low demand. On the other hand, controllers can also sometimes manage to depart aircraft with a separation less than the target level, depending on factors such as the availability of multiple runways for departure. In this case, each second less than the target separation level is counted as a second *gained*. Then, the Departure Spacing Efficiency in each 15 minute interval is given by:

$$\eta = 1.00 + \frac{\text{Total seconds gained in the interval} - \text{Total seconds lost in the interval}}{\text{Length of interval}}$$

It should be noted that the use of multiple runways does not always allow departures to take place with less than the target level of spacing. For example, at Boston, departure operations on runways 22R and 22L have to take place as on a single runway, because both sets of departures have to use the same departure fixes. However, when runways 4R and 9 are used for departures, aircraft can be spaced more closely,

thus boosting the airport's efficiency. Figure 3-9 demonstrates the calculation procedure for counting the time lost in a 15 minute interval. The local time is shown on the X axis. Each spike denotes the wheels-off time for a departure, with the height of the spike corresponding to the weight class of the aircraft. The spike then tapers off, reaching the 'clear to release' line when the target separation interval elapses. The gap from this point to the next departure spike counts towards the total number of seconds lost in the current 15 minute interval. There is, however, a caveat associated

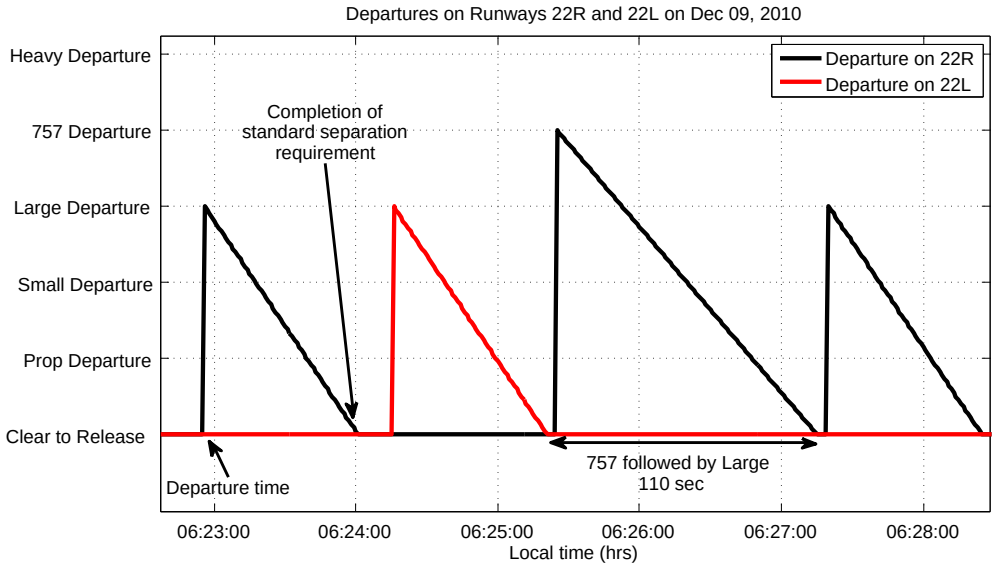

Figure 3-9: Visualization of departures

with calculation of the total time lost. As described previously, arrival spacing is not under the discretion of Boston Tower. In configurations where arrivals take place on a runway that is the same as or that intersects the departure runway, this can cause a dip in the efficiency. We account for this effect by discounting the idle time of a departure runway when an arrival is on short final (within 2.5 nm of threshold) to an intersecting runway or to the same runway. Figures 3-10 and 3-11 show the variation of Departure Spacing Efficiency with the time of day for December 09, 2010, with and without accounting for the arrival effect, respectively. In each figure, the plot on the top shows the efficiency in each 15 minute interval, while the plot on the bottom shows the departure count in the corresponding intervals. The colored bars in the middle indicate the departure demand level at the airport, calculated using

a combination of the departure counts and queue lengths. We note that there are several time periods (for example, between 1630 and 2015 hours), when not including the impact of arrivals would lead to the erroneous conclusion that the efficiency was lower than it actually was. A comparison of Figures 3-10 and 3-11 suggests that the efficiency during this time was above 85% when accounting for arrivals, whereas it was as low as 75% when the effect of arrivals was ignored.

Note the large dip in efficiency just prior to the configuration change at 1000 hours. A few intervals with net efficiency more than 1.0 can also be seen. These intervals correspond to spikes in the departure count, since consistent separation values less than the target level result in a large number of departures. The most notable high-efficiency interval is the one from 1945 to 2000, which is in the middle of a period with high demand. The bottom plot shows that the controllers managed 10 departures in this interval (nine on runway 33L and one on runway 27), while a comparison with Figure 3-6 shows that 7 arrivals were also achieved. In this way, a combination of different performance metrics offers insights into the intricacies of surface operations, that result in the net operational counts that are the traditional measure of airport performance.

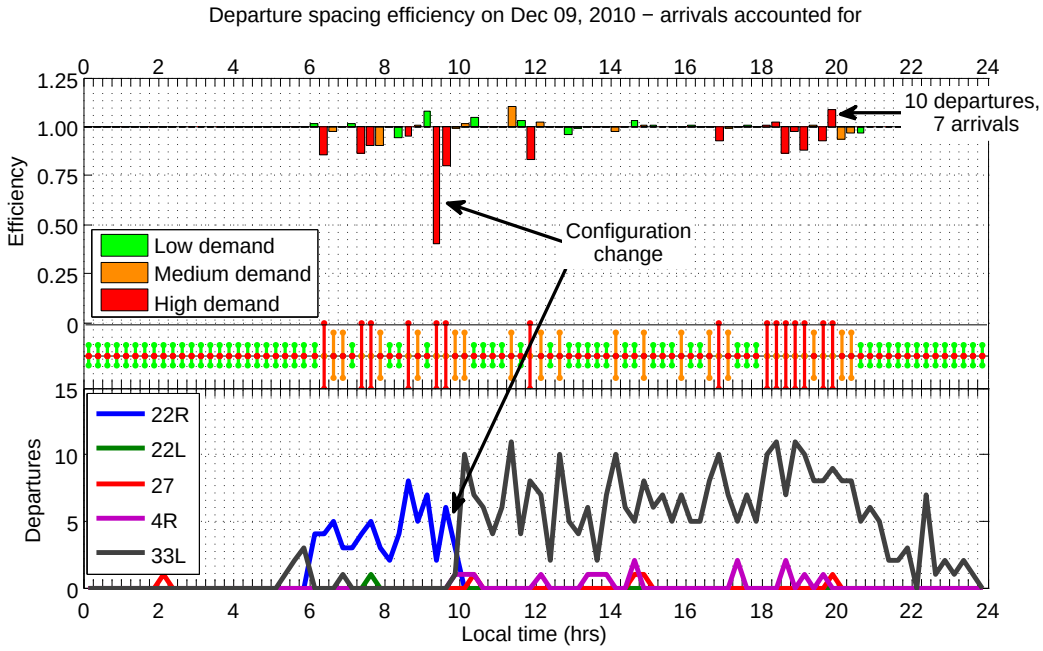

Figure 3-10: Departure spacing efficiency on Dec 09, 2010, accounting for the effect of arrivals on the same/crossing runway.

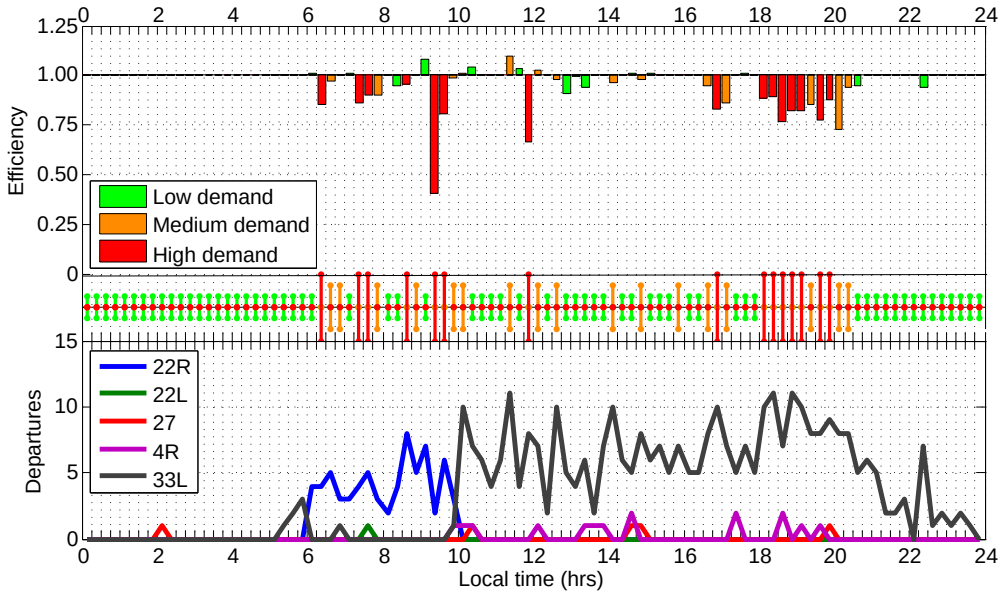

Figure 3-11: Departure spacing efficiency on Dec 09, 2010, not accounting for the effect of arrivals on the same/crossing runway.

3.4 Performance Metrics: Operational Feedback

The metrics defined above, tracked over several months of data, can be used to measure average operational performance. For example, Figure 3-12 shows the average departure spacing efficiency at Boston, sorted by configuration and demand level. One immediate conclusion from the figure is that for most configurations, the efficiency drops as demand increases. This is intuitive, since high demand usually means more complex operations, more runway crossings, and so on. We can also see that departures on runways 9 and 4R is the most efficient configuration. As mentioned before, this configuration allows closely-spaced departures on the two crossing runways, which boosts the efficiency. An interesting footnote is that the 33L | 27 configuration, with departures on runway 27, is more efficient than the 27 | 33L configuration. Either of these can be used when winds are from the northwest. Therefore, Boston ATC now prefers using the former configuration when the departure demand is high, particularly in the morning, when this is not accompanied by high arrival demand. According to the Boston Air Traffic Manager, one possible explanation for the in-

creased spacing on 33L could be that it is longer than runway 27. This means that a departure takes longer to be completely clear of the runway, which is a visual cue for the controller to release the next aircraft.

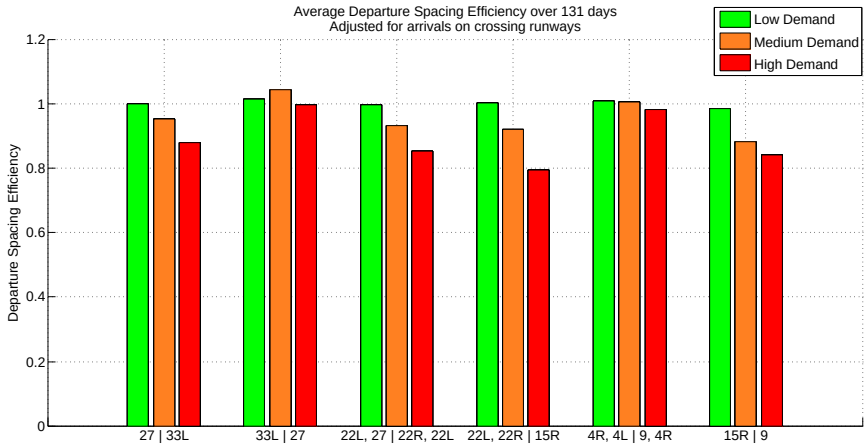

Figure 3-12: Average Departure Spacing Efficiency in common configurations

3.5 Summary

This chapter presented several ways in which surface surveillance data could be used for the detailed analysis of airport surface operations. This included directly measurable quantities like departure queue statistics and throughput characteristics, along with performance metrics like average taxi-out times, runway utilization and departure spacing efficiency. The ensuing discussion showed how they could be used to gain insight into the performance of the airport.

Chapter 4

Taxi Time Prediction

4.1 Introduction

4.1.1 Motivation

A significant portion of total flight delay is absorbed on the airport surface, before departure. Therefore, reduction of taxi-out times has the potential to substantially reduce delays and fuel consumption on the airport surface. Prediction of taxi-out times is a necessary component of any proposed algorithm to reduce departure delays [18]. Previous studies have used regression techniques [21, 22] or queuing models [17, 23] to predict taxi-out times. These methods make use of Aviation System Performance Metrics (ASPM) data [15]. This data set lists only the gate-out and wheels-off times for each aircraft, and consequently, it does not offer any opportunity to investigate the interaction between aircraft on the surface. In addition, it is not accurate for general aviation flights. Other systems, such as NASA's Surface Management System, are capable of real-time tracking of surface movement, but still use logit models built from aggregated data to predict taxi-out times [24]. Besides the characterization of airport operations, ASDE-X data can also be used for prediction purposes, as detailed in this chapter.

4.1.2 Prediction Model Overview

The algorithm described here predicts taxi-out times based on a network model of the airport surface. Such models have been previously proposed for urban Operations Research problems, and there exists literature that deals with solving optimal route problems in this context [25, 26]. The urban transportation network concept has been adadpted in this chapter, to handle aircraft taxi-out operations, by modeling the time taken by aircraft to taxi over each taxiway link as a random variable. A set of theoretical distributions is fitted to the observed empirical data on link travel times: the modeled distributions are determined so as to minimize the Kullback-Leibler distance (an information-theoretic measure of the 'distance' between two probability distributions) between the modeled and observed probability distributions. This theoretical model, augmented by knowledge of the current state of traffic on the surface, is then used to predict taxi-out times for each aircraft. All the results presented here use 20 days of ASDE-X data for training the model, and 20 different days of data for validating the model.

4.2 Model Development

4.2.1 Model Structure

Figure 4-1 shows the set of runways and taxiways on the airport surface that are represented in the network model. The taxiways form the links of the network, and their major intersections are marked as the nodes. The taxi-out phase for an aircraft is defined to be from the time an aircraft leaves the gate to the time it starts its takeoff roll from the runway threshold. Therefore, the potential source nodes in the network are the ones adjoining the gates, while the potential terminal nodes are the runway thresholds. The objective is to predict the time required by each departing aircraft to travel from its source node to its terminal node. An abstraction of the resulting model is shown in Figure 4-2. Note that Figure 4-2 shows the union of the networks for all possible airport configurations (allocations of runways to landings and takeoffs). In

Figure 4-1: Layout of the airport surface at Boston Logan. Nodes in the network model are marked with white boxes. The configuration-specific network for departures from Runway 33L has been highlighted.

practice, only one configuration is active at a time, and each aircraft has only one source node and one terminal node. BOS typically operates in configurations with only one primary departure runway, but the proposed model can be easily extended to other airports with multiple runway queues. Figure 4-3 shows the specific network for departures from Runway 33L. In any specific configuration, aircraft maintain a flow from the terminal to the runway, and generally do not taxi in cyclic paths. Consequently, the configuration-specific networks are directed acyclic graphs with random link travel times.

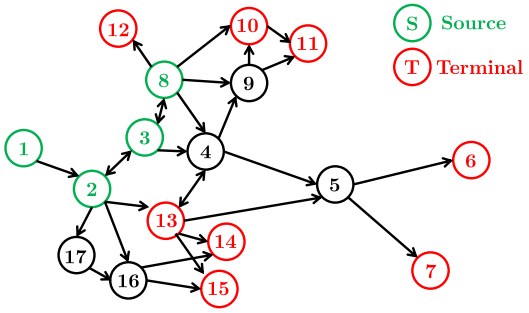

Figure 4-2: Abstraction of the airport surface as the union of all configuration-specific networks, with link directionality marked. Green nodes are potential sources and red ones are potential terminal nodes.

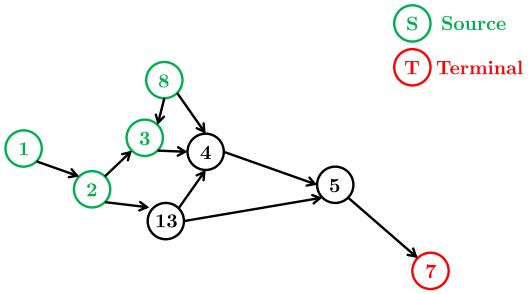

Figure 4-3: Network layout for departures from Runway 33L.

4.2.2 Analysis of Empirical Data

Figure 4-4 shows the procedure adopted for determining the empirical distributions of travel times for each individual link. The time required to travel from node to node by each flight in the training data set was logged. The set of travel times between each ordered pair of nodes was used to generate the aggregate empirical distributions. It should be noted that 'link travel time' was calculated from the instant a flight exited one node, to the instant it entered the next node on its path. The distribution of time spent within each node was tracked separately.

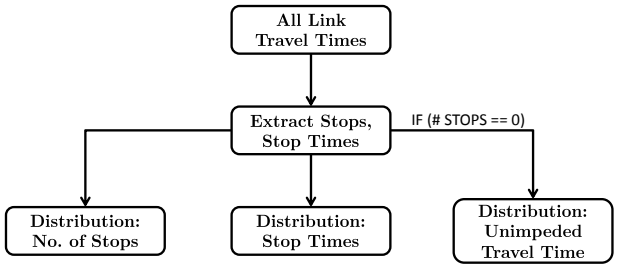

Figure 4-4: Flowchart for measuring empirical distribution of link travel times.

From the instantaneous velocity information in the data, each instance of link transit was classified as *impeded* or *unimpeded*. A flight was defined to have passed 'unimpeded' through a link if the velocity of that flight never dropped below 2 m/s on that particular link. The velocity threshold was based upon the full distribution of taxi velocity over each link, which showed a marked distinction at 2 m/s. Figure 4-5

shows an example for the link 1→2. It can be seen that the most frequent velocity values are below 2 m/s, or in a band around 7 m/s. The instances of unimpeded transit were used to generate the unimpeded taxi-time distribution over each link. The flights that were impeded were further analyzed to extract the distribution of number of stops during the transit, and also the distribution of stop times.

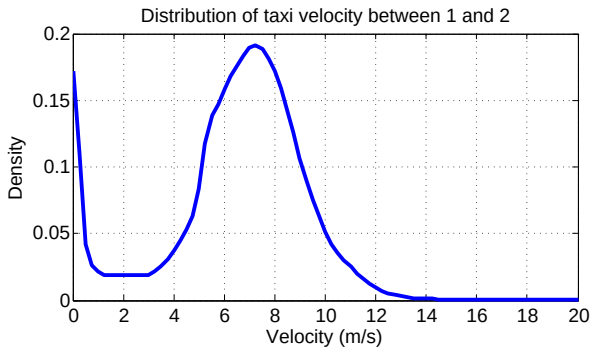

Figure 4-5: Distribution of taxi velocity over the link 1→2.

4.2.3 Link Travel Time Model

The resulting empirical distributions were analyzed with a view to fitting explanatory theoretical models. The unimpeded travel time distribution over each link was modeled by an Erlang random variable, with parameter λ and order n. The distribution of number of stops on each link was modeled as a geometric random variable with parameter p, while the time distribution of each stop was modeled as an exponential random variable with parameter μ. Figures 4-6 to 4-8 show a comparison between the theoretical and empirical distributions for the link 1→2. The parameters of the random processes underlying each link were tuned by minimizing the Kullback-Leibler (KL) Divergence [27] between the empirical and theoretical distributions. KL divergence is a measure of the 'distance' between two probability densities, and minimizing it is one way of ensuring a good fit between the theoretical model and empirical observation.

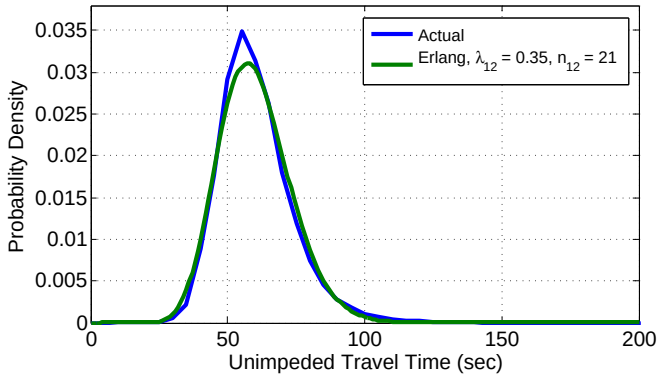

Figure 4-6: Unimpeded travel time over the link 1→2.

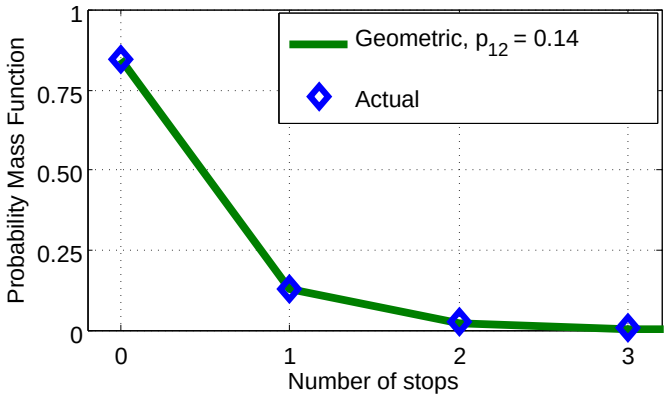

Figure 4-7: Distribution of number of stops over the link 1→2.

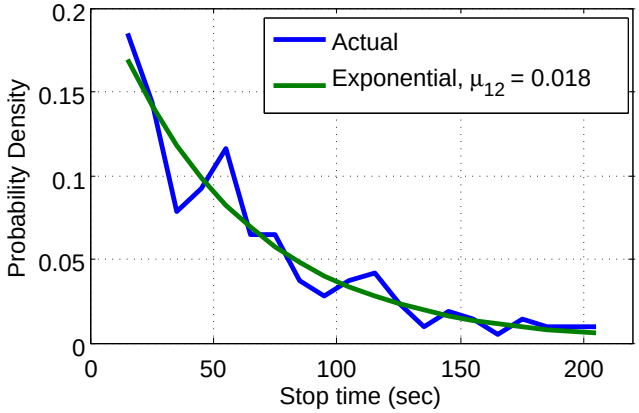

Figure 4-8: Distribution of stop times over the link 1→2.

In summary, the model generated by the estimation procedure implies that the travel time over a link $A \rightarrow B$, e_{AB}, is given by the sum of an Erlang random variable and a geometric number of exponential random variables. The Erlang denotes unimpeded travel over the link. In addition, there is a delay term containing a random number of stops, each of which is distributed like an exponential random variable with parameter μ_{AB}. The probability of each additional stop is p_{AB}. The resulting model is given by Equation (4.1), where $m = \{0, 1, ...\}$ is a geometric random variable with parameter p_{AB}.

$$e_{AB} = \text{Erlang}(\lambda_{AB}, n_{AB}) + \sum \underbrace{\text{Exp}(\mu_{AB})}_{m \text{ instances}} \tag{4.1}$$

Taking expectations of both sides of (4.1), and noting that the number of stops is independent of the individual stop times, we get Equation (4.2), which gives the mean travel time over each link.

$$E[e_{AB}] = \frac{n_{AB}}{\lambda_{AB}} + \frac{p_{AB}}{1 - p_{AB}} \cdot \frac{1}{\mu_{AB}} \tag{4.2}$$

4.3 Results

4.3.1 Aggregate Predictions

As mentioned before, the parameters of the travel time distribution model were tuned for each link. The range of parameters observed over all links is listed in Table 4.1. To calculate the full distribution of link travel times using Equation (4.1), it is necessary to carry out a convolution of the Erlang and the random number of exponential random variables. Note that the parameters of the unimpeded Erlang and the stop-time exponentials are different, which means that the convolution is not an Erlang of higher order and has to be done numerically. However, conditioned on the number of stops m, the exponentials among themselves form an Erlang with parameter μ_{AB} and order m. Therefore, the net distribution could be calculated as a weighted sum of the individual distributions, conditioned on the number of stops. For computational

Table 4.1: Parameter ranges for theoretical distributions.

Link-specific variable	Value	Range
Stopping probability	p_{AB}	[0.1, 0.5]
Mean number of stops	$\frac{p_{AB}}{1-p_{AB}}$	[0.11, 1.00]
Stop time parameter	μ_{AB}	[0.012, 0.025]
Mean time of stop (sec)	$\frac{1}{\mu_{AB}}$	[40, 83]
Unimpeded Erlang rate	λ_{AB}	[0.16, 0.45]
Unimpeded Erlang order	n_{AB}	[12, 30]
Mean unimpeded time (sec)	$\frac{n_{AB}}{\lambda_{AB}}$	[60, 120]

purposes, this number m was limited to a maximum value of 3, since the probability of stopping more than 3 times on any single link is very small.

The component travel time distributions for link 1→2, conditional on the number of stops on the link, are shown in Figure 4-9. Each empirical conditional distribution is compared with the corresponding model prediction in Figures 4-10 to 4-12. The sum of these theoretical distributions, each weighted by the probability of stopping on the link for the corresponding number of times, is the full predicted distribution of travel time over the link. A comparison of the model prediction and the actual realized distribution, from the test data, is shown in Figure 4-13. It should be emphasized that the model parameters were tuned using the training data set, while the realized distribution in Figure 4-13 is from a separate set of test data. It can be seen that the model prediction is close to the realized distribution, and is especially good in the tail region.

The tuned values of distribution parameters for each link offer interesting insights into the operational characteristics of the airport. Some sample values are given in Table 4.2. For example, the mean unimpeded travel time over each link, given by the ratio n/λ, can be thought of as the ratio of a distance metric (n) to a velocity metric (λ). This is borne out by the parameter values, with long links tending to have higher-order Erlang distributions than short links. In addition, the final links leading to runway thresholds, which is when pilots finish the final checks before takeoff,

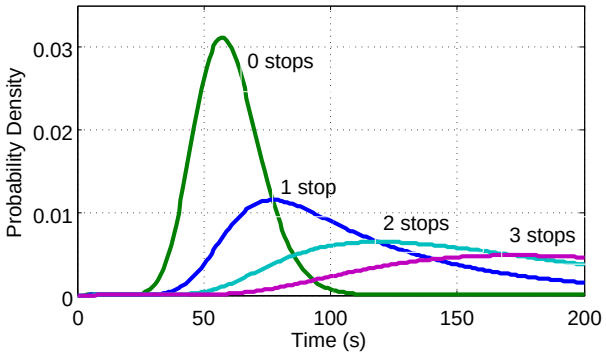

Figure 4-9: Component conditional distributions for travel over link 1→2

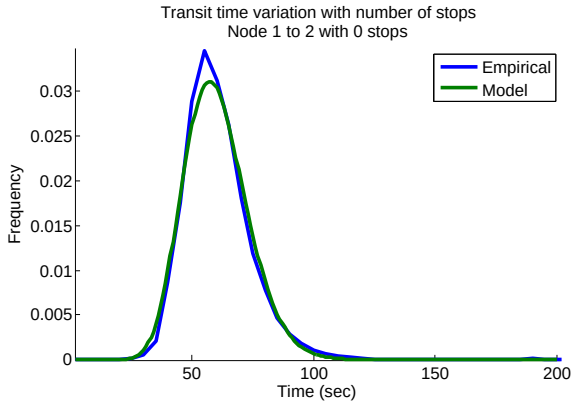

Figure 4-10: Comparison of travel time distributions with 0 stops

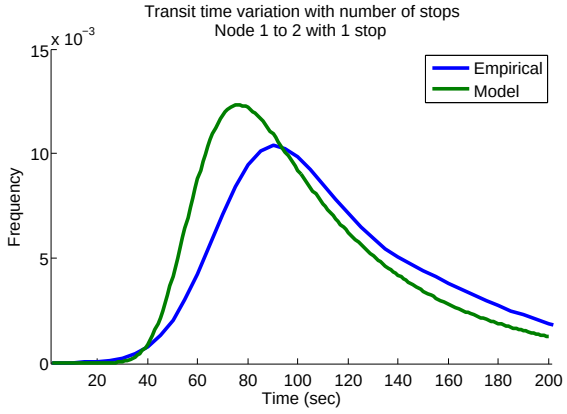

Figure 4-11: Comparison of travel time distributions with 1 stop

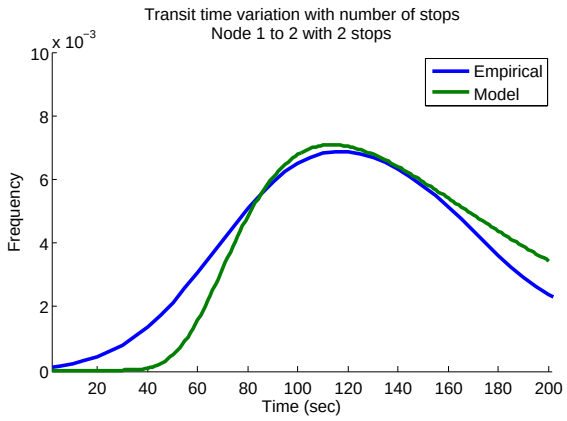

Figure 4-12: Comparison of travel time distributions with 2 stops

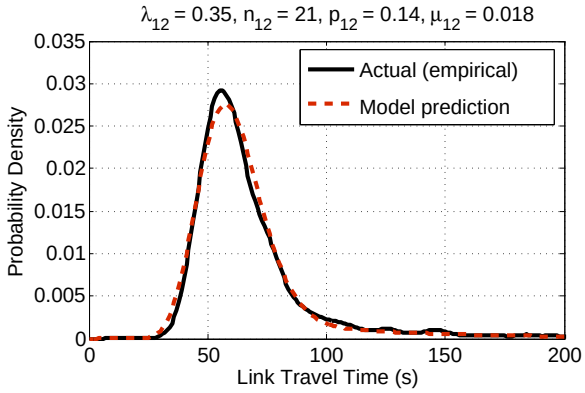

Figure 4-13: Comparison of full travel time distributions over link 1→2

generally have lower λ values than links deep inside the network. This means that the model has recognized, from the training data, that unimpeded velocities on the links leading to the runway threshold tend to be lower than those near the terminals. The parameters of the exponential random variables offer insights into the trend of stop times on each link. Specifically, the quantity $1/\mu$ is the mean time of a stop on the link. This tends to be between 20 and 100 seconds. Again, μ values tend to be lower on the final links, which means that the links that contain departure queues have longer stops than others.

Table 4.2: Parameter values for some sample links.

Link	λ	n	μ	p
1→2	0.35	21	0.018	0.14
2→3	0.31	18	0.016	0.11
8→3	0.31	21	0.022	0.11
4→5	0.26	20	0.019	0.23
5→6	0.22	27	0.016	0.48
9→10	0.20	18	0.016	0.50

4.3.2 Traffic-dependent parameters

The average probability of stopping on each link varies between 0.1 and 0.5, which means that on any link, between 10% and 50% of flights stop at least once. Since the distribution is geometric, the probability of stopping again remains unchanged even if a flight has already stopped once. This is intuitively consistent, considering that aircraft usually have to stop during taxi-out because of conflicts with other aircraft. Given that an aircraft has had to stop to let another aircraft cross its path should have no bearing on the probability of encountering another aircraft while on the same taxiway. Although the parameter p_{AB} is constant for a given flight, it turns out that its value is a function of the current state of traffic on the surface. For example, Figure 4-14 shows the variation of mean travel times over link 1→2, with the traffic on the surface. The X axis denotes the number of active departing aircraft (those that have

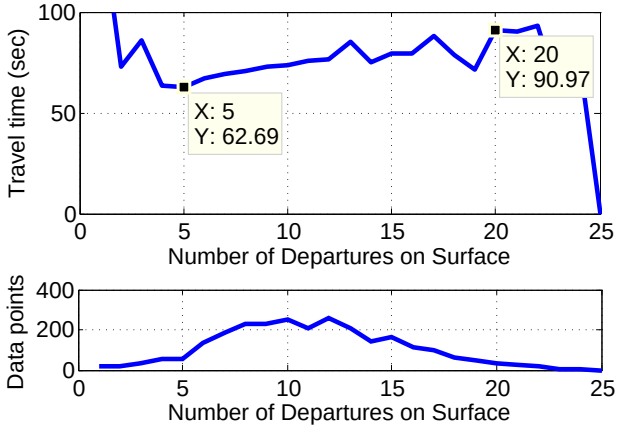

Figure 4-14: Variation of travel times over link 1→2 with traffic on the surface.

pushed back from the gate but have not taken off) at the moment an aircraft left node 1 for node 2. The Y axis is the mean travel time for all flights that traveled from node 1 to node 2 when the traffic was at the corresponding level. It can be seen that there is a clear increase in travel times as congestion on the surface increases. Therefore, we modeled the stopping probability as a function of the number (N) of active departing aircraft on the surface. This was calculated by assuming that the other parameters in the distribution (unimpeded travel time and time for each stop) remain constant, while the stopping probability varies. By measuring the left-hand side of Equation (4.2) conditioned on N, we can solve for the conditional stopping probability:

$$p_{AB,N} = \frac{\mu(E[e_{AB,N}] - n_{AB}/\lambda_{AB})}{1 + \mu(E[e_{AB,N}] - n_{AB}/\lambda_{AB})}. \tag{4.3}$$

Here, the expectation value is measured empirically. Figures 4-15 and 4-16 show the variation of calculated stopping probability with surface traffic for two links. Link 1→2 is near the gates, while link 5→7 is near Runway 33L (refer Figure 4-1). Note that the values have been smoothed using a heuristic such that only points that have sufficient data are used for curve fitting. It can be seen that for link 1→2, stopping probability is very low when traffic is sparse. On the other hand, a significant fraction of flights tend to stop on link 5→7 even during light traffic conditions. When traffic is heavy, an aircraft using the link 5→7 is likely to stop on it at least once with high probability, and quite likely more than once. This behavior can be explained by the observation that the link holds the departure queue when runway 33L is active. During heavy traffic conditions, there is a large queue of aircraft waiting to depart, thereby causing every flight to move in a stop-start fashion.

4.3.3 Taxi-out time predictions

Once the distributions of travel times over individual links are available, it is possible to make predictions of full taxi-out times for each aircraft. These predictions are based on knowledge of the proposed taxi path, and the current state of traffic on the surface. The proposed taxi path is assumed to be available before the start of

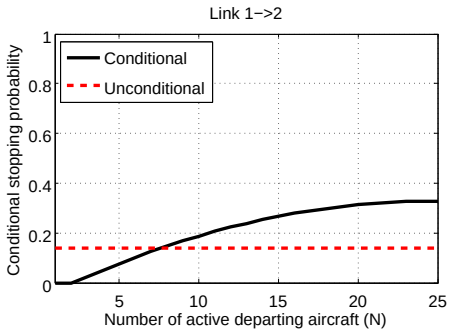

Figure 4-15: Variation of stopping probability over link 1→2 as a function of the departure traffic on the surface.

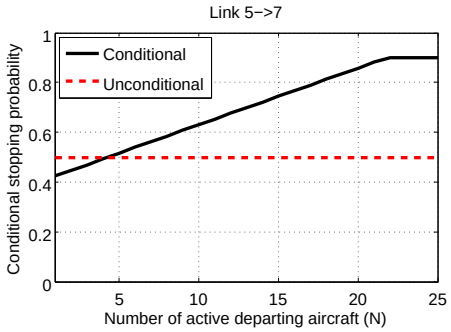

Figure 4-16: Variation of stopping probability over link 5→7 as a function of the departure traffic on the surface.

taxi, based on observations carried out in the Air Traffic Control Tower at Boston Logan. The current state of surface traffic is tracked using ASDE-X data. The model makes predictions of taxi-out times using the expectation values based on Equation (4.2), in which the value of stopping probability p_{AB} for each link is the conditional value estimated using Equation (4.3). For every additional aircraft in the departure queue, a fixed time penalty is imposed on all the aicraft expected to be behind it. The algorithm for real-time predictions is described below:

Start

1: **for all** time instants t **do**

2: **for all** aircraft i detected in any node n at time t **do**

3: **if**

4: Aircraft i detected for the first time **then**

5: Calculate expected arrival time at departure queue (t_{ai}) by adding the expected travel times over each link and node on its path, except last link

6: Using expected number of aircraft already in queue at t_{ai}, predict departure time t_{di} of aircraft i

7: Augment expected departure queue length between t_{ai} and t_{di} by one

8: **else**

9: Subtract 1 from the expected departure queue length between t_{ai} and t_{di}

10: Update expected t_{ai} by adding the expected travel times over all remaining links and nodes on its path, except last link

11: Using expected number of aircraft already in queue at the new t_{ai}, update departure time t_{di} of aircraft i

12: Augment expected departure queue length between new t_{ai} and t_{di} by one

13: **end if**

14: **end for**

15: **end for**

End

The update steps (10) and (11) adjust for two stochastic factors in the taxi-out process: (i) the time taken by the aircraft to travel over the previous link may be different from the prediction, and (ii) the expected queue arrival times of other aircraft on the surface (and hence the expected queue size seen by the current aircraft) could have changed, based on their own prediction updates. Figures 4-17 and 4-18 show the results from this algorithm over an entire day. The X axis in the plots on top is the local time at Boston, while the Y axis is the taxi-out time (predicted and actual) in seconds. The plots on the bottom show the distribution of prediction error over the whole day. Each red circle is the taxi-out time for a real flight on that day, with the X coordinate denoting its departure time. The green circles at the same X locations are the corresponding predictions. In Figure 4-17, all calculations are carried out assuming that link travel times are independent of the current traffic level. The predicted link travel times are thus equal to their *static* or unconditional means. Since the expected queue size seen by each aircraft is still calculated, some of

the effect of congestion is accounted for by larger predicted times in queue. However, this does not account for all the additional delay absorbed by aircraft on the surface. Specifically, the 'static means' prediction method does not compensate for the effect of the greater probability of conflicts on the surface. Consequently, it can be seen that during peak times, the predictions do not track actual taxi-out times very well. This leads to a significant increase in the proportion of under-predicted taxi-out times, as shown in the bottom plot of Figure 4-17. On the other hand, Figure 4-18 shows the predictions produced by assuming that the parameter p_{AB} varies with surface traffic. This method, which uses *dynamic* or conditional means, can be seen to track actual taxi-out times much better in the peak periods.

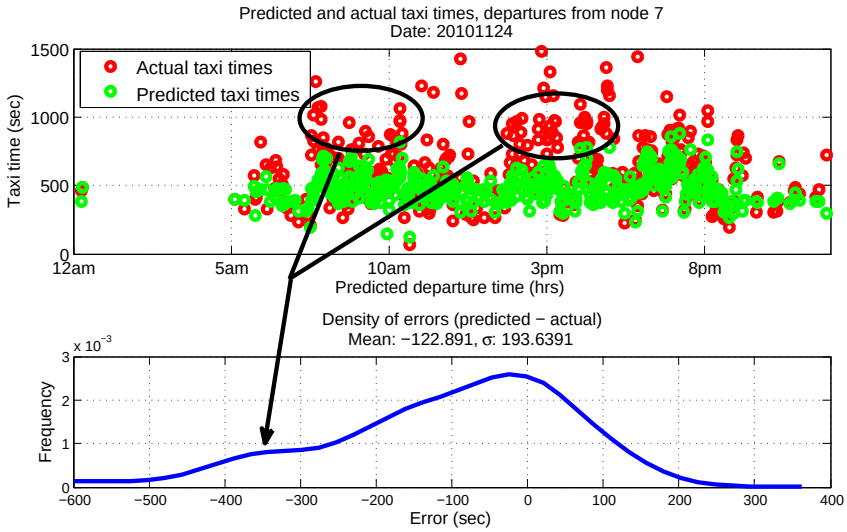

Figure 4-17: Prediction of taxi-out times on Nov 24, 2010 using static means. The expected travel time over each link up to the departure queue is assumed independent of current traffic level.

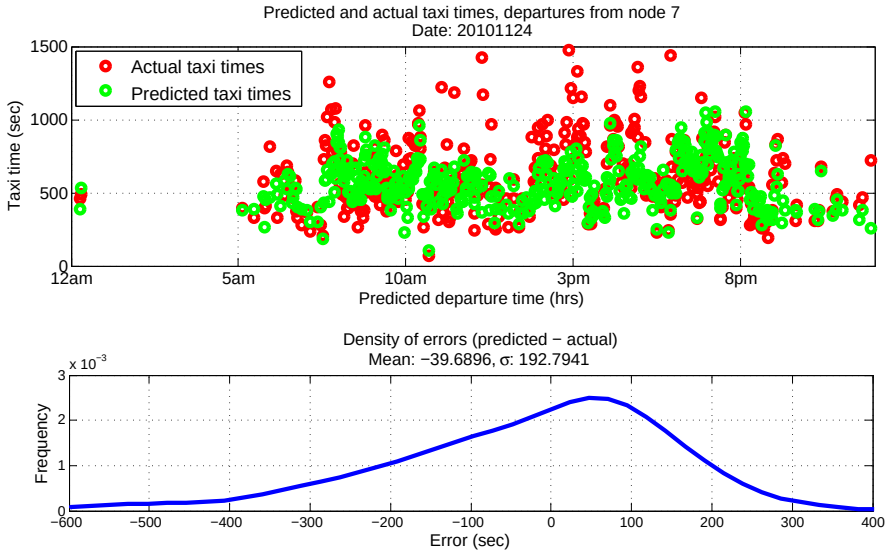

Figure 4-18: Prediction of taxi-out times on Nov 24, 2010 using dynamic means. The expected travel time over each link up to the departure queue is a function of current traffic level.

4.3.4 Prediction accuracy for complete taxi-out times

Aggregate prediction results from the model are shown in Figure 4-19 for departures from Runway 33L. It shows the distribution of prediction errors over 20 days from an independent test data set. The prediction values used were the ones generated upon first detection of each aircraft, that is, around time of pushback. The mean error is an under-prediction of 39 seconds, with a standard deviation of 192 sec. It was found that 70% of all predictions were within ±3 minutes of actual taxi-out times. This level of performance is typical across all configurations, and is better compared to an error standard deviation of 5 minutes (300 sec) reported in literature [23].

Figure 4-20 shows the improvement in prediction accuracy from successive nodes on a particular taxi path. The plot shows the distribution of prediction error from each node, based on all flights that used the particular taxi path over the 20 days of test data. It can be seen that the error variance decreases, and the prediction becomes more accurate, as the flights move closer and closer to their terminal nodes. Another point of note is that the distribution tails on the negative side (under-prediction) are fatter than the ones on the positive side (over-prediction). The positive errors are a

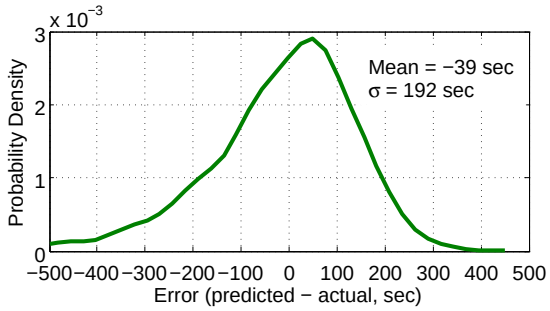

Figure 4-19: Distribution of full taxi-out time prediction error from 20 test days, for departures from Runway 33L.

result of the stochastic nature of the taxi-out process, which is captured well by the prediction model. On the other hand, unusually high taxi times may be the result of external events, such as delays due to runway closures, fixed departure times due to constraints in other parts of the National Airspace System, etc. These events are not captured by the current model formulation.

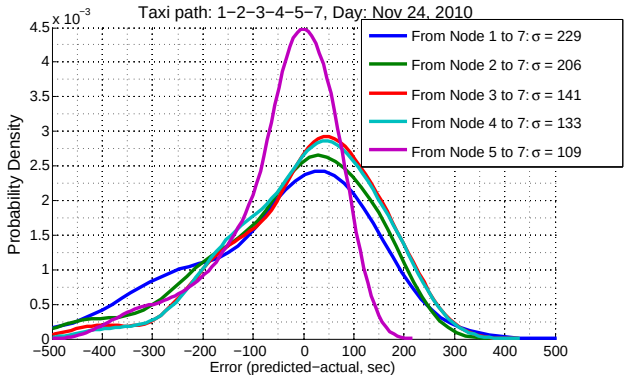

Figure 4-20: Improvement in error variance along successive nodes on a taxi-out path

4.3.5 Recommendation of taxi-out start times

It is possible to use the taxi-out time prediction model for recommending taxi-out start times (that is, pushback times) for individual aircraft. Figure 4-21 shows a simple version of the procedure devised to make suggestions for specific flights. The X axis shows the range of times over which the search for the best start time was carried out. These are within ± 5 minutes of the actual start time for that flight. The

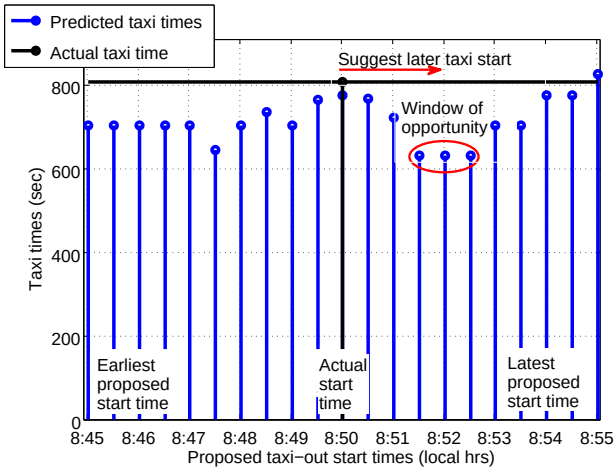

Figure 4-21: Recommendation of taxi-out start time for a sample flight.

height of the black bar corresponds to the actual taxi-out time for the flight. The blue bars represent the full gate-to-runway predictions, corresponding to the start times on the X axis. Since the state of traffic on the surface is constantly changing, the model produces different taxi-out time predictions for different proposed start times. Looking at the full set of predictions makes it possible to identify the best taxi start time for the flight. In the example shown, leaving at 8:52 am instead of 8:50 am would have potentially reduced the taxi-out time by 150 seconds.

4.4 Summary

In this chapter, a model for prediction of aircraft taxi-out times based on detailed surface surveillance data, was presented. It was showed that abstraction of the airport surface as a network facilitates the definition of a theoretical model to explain the taxi-out process. The link travel times were modeled as a sum of two random variables: an unimpeded travel time and a delay component. The parameters of the distributions of the random variables were determined so as to minimize the Kullback-Leibler distances between the model and the empirical distributions. The model works very well as a prediction tool in the aggregate sense, matching the observed empirical distributions of link travel times with high accuracy. Full taxi-out time predictions are made, with an error standard deviation of approximately 3 minutes.

Chapter 5

Fuel Burn Modeling

5.1 Introduction

Estimation of aircraft fuel burn plays an important role in determining the environmental impact of air traffic operations as well as in estimating the benefits of efficiency-enhancing procedures, and has been a topic of interest to the research community for several years [28]. Taxi-out fuel consumption is most often determined using the fuel burn indices presented in the International Civil Aviation Organization (ICAO) engine emissions databank [29]. The ICAO fuel burn indices provide fuel burn rates for only four engine power settings (corresponding to 7% or taxi/idle, 30% or approach, 85% or climb-out, and 100% or takeoff), and are based on estimates provided by engine manufacturers [30]. Recently published studies [31, 32] have shown that the ICAO estimates can be quite different from the actual fuel burn, when considering the departure flight phase in the terminal area. The terminal area fuel burn considered in these studies includes the fuel consumed during taxi-out as well as the initial part of the climb. In contrast, in order to estimate the benefits of surface traffic management strategies [17], it is necessary to have accurate estimates of the taxi-out (on-surface) fuel burn. Since fuel flow rates in the airborne flight phase are much higher than during taxi-out, total departure fuel burn may not be a good indicator of surface fuel burn. Also, a large part of total flight delay is absorbed on the ground, before departure. To quantify the impact of this delay, it is necessary to have an

estimate of the fuel burn associated with surface trajectories of departing aircraft. Previous studies on this topic [2] have used the ICAO fuel burn indices (augmented with physical models) to translate the surface trajectories into fuel burn estimates, and may therefore not be representative of operational aircraft. It appears that this work is the first attempt to develop models of surface fuel burn using Flight Data Recorder archives from an actual, operational fleet.

5.1.1 Problem Description

The high-level objective of this work is build a model that, when given the surface taxi trajectory of a flight (for example, from a surface surveillance system such as the Airport Surface Detection Equipment - Model X, or ASDE-X) [1], can form an accurate estimate of its fuel burn. This model can then be utilized in a taxi-out departure tool with the objective to minimize the total fuel burn impact of surface operations at an airport. Since the results of any optimization process hinge upon accurate estimation of all the involved variables, it is necessary that the fuel burn model be as close to the actual fuel burn as possible. In order to build such a model, we need to estimate fuel consumption from estimates of aircraft position, velocity and acceleration. One method for doing so is to divide the surface trajectory into different taxi phases (for example, stops, turns, constant velocity taxi, etc.), to estimate the engine power settings for each of these phases (using physics-based models and pilot surveys), interpolate/extrapolate ICAO fuel burn indices to these power settings, and to use these estimated fuel burn indices to determine the fuel consumption of the trajectory [2].

However, several factors confound such an estimation using ICAO data alone. Firstly, the ICAO fuel burn estimates provided by engine manufacturers may not reflect the characteristics of the engines in the operational fleet which are subject to frequent use. Secondly, the engines are staged and tested only at four power settings, and in particular, 7% may not be representative of the typical power setting during taxi. Thirdly, pilot behavior is a critical factor in determining the power settings during the different taxi modes: for example, some pilots may not change

their power settings when they stop, or when they accelerate from a stop, choosing instead to "ride the brakes". Idealized models of taxiing cannot capture this behavior, or even the average. Finally, several studies have shown a nonlinear dependence of fuel flow rate on engine power settings, and the relationship at low power settings is not well-understood. Therefore, caution must be extended in interpolating or extrapolating fuel burn indices at low power settings (such as near ground idle). In order to overcome these challenges, we adopt a data-driven approach to estimating the fuel burn of surface trajectories, using Flight Data Recorder (FDR) archives.

5.1.2 FDR Database

The Flight Data Recorder (FDR) is a device onboard commercial aircraft that stores the history of several parameters such as aircraft position, velocity, fuel flow rate, ambient and engine temperature, and so on. FDR archives from over 2300 flights belonging to a former international airline were used for the purposes of modeling and validation in this study. The dataset included flights originating from the US, Europe, Asia and Africa. Aircraft types included in the dataset were the Airbus A320 family (A319, A320, A321), the A330 family (with Rolls Royce and General Electric engines) and the A340, the Avro RJ85 and Boeing's B757, B767 and B777. A full list of aircraft and engine types, along with their Maximum Takeoff Weight (MTOW), is shown in Table 5.1.

Table 5.1: Aircraft types and Engines

Type	Engine	Number of Engines	Number of Flights	MTOW (kg)
A319	CFM56-5B5-2	2	140	64,000
A320	CFM56-5B4-2	2	238	73,500
A321	CFM56-5B1-2	2	174	83,000
A330-202	CF6-80E1A4	2	224	230,000
A330-243	RR Trent 772B-60	2	237	230,000
A340-500	RR Trent 553-61	4	260	372,000
ARJ85	LF507-1F	4	263	44,000
B757	RR RB211-535E4	2	178	106,600
B767	P&W 4060	2	285	186,900
B777	GE90	2	364	344,550

A total of 105 parameters were available in the dataset, of which the ones of primary interest to us were the fuel flow rate, throttle setting, velocity, position (latitude/longitude), ambient temperature, thrust and engine fan speed (N1). It is believed that some of these quantities, such as the thrust, were derived estimates and not actual measurements.

5.2 Data Analysis Algorithms

5.2.1 Preprocessing

Raw data was run through multiple preprocessing algorithms for the purposes of analysis. These steps included sorting of flights, removal of the airborne phase, filtering of the velocity estimates, and the extraction of events of interest such as stops and turns. The velocity as derived from position required filtering due to the relatively low data update rate during taxi-out (Table 5.2). Since the noise level was low, a linear Kalman filter was found to be sufficient.

Finally, the taxi-out phase was separated by extracting the portion of the surface trajectory after pushback from the gate and before commencement of the takeoff roll. Identification of pushback was carried out using a combination of fuel-flow rate and speed conditions, and the start of the takeoff roll was determined using a speed cut-off.

5.2.2 Baseline Fuel Consumption

The ICAO procedure for estimation of taxi-out fuel burn assumes that taxi operations occur entirely at idle thrust (the 7% power setting), and thus proposes the use of

Table 5.2: Dataset update rates

Flight Phase	Update Rate
Taxi	5 sec
Takeoff/Landing Roll	1 sec
Climb/Descent	10 sec
Cruise	150 sec

constant rated idle thrust fuel flow for all calculations [29]. It defines the fuel burn index to be the fuel flow rate per engine at idle thrust. The version of the ICAO database used for this study was from December 2010 [33]. To compare these numbers to actual data, the average fuel flow rate for each available aircraft type in the dataset was calculated, by dividing the taxi-out fuel burn by the taxi-out time and the number of engines, and averaging this over all aircraft of a given type. As seen from Figure 5-1, the ICAO fuel burn index is not necessarily a reflection of the true per-engine fuel burn rate. The comparison shown in this figure is in agreement with the results from a previous study [32], where a comparison of *total* average fuel flow rate is available. It can be seen that in several cases, the ICAO method produces an overestimate of fuel burn. This result is important from the point of view of estimates that drive environmental policy, such as the quantification of total CO_2 emissions at airports.

There are several possible reasons for the differences observed here. These include the fact that the ICAO numbers are produced from testbed engines in idealized conditions, while the FDR data is from mounted and operational engines. Ambient conditions also affect fuel consumption. In addition to this, there are human factor elements such as pilot behavior. Since the objective is to estimate fuel consumption for real-world taxi operations, it is important to account for such effects as best as possible.

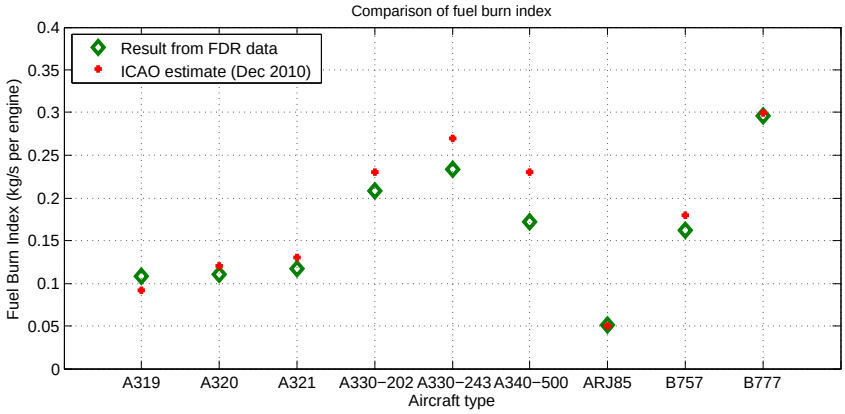

Figure 5-1: Comparison of fuel burn index as calculated from FDR data and that obtained from ICAO.

5.2.3 Events of Interest during Taxi-out

The surface trajectory is composed of periods of constant velocity taxi in a straight line, interspersed by events such as stops and turns. The results of any estimation procedure that incorporates these events will likely be influenced by their exact definitions. Therefore, the algorithms used to detect the number of turns and stops during taxi-out, as used in this study, are discussed below.

Detection of number of turns during taxi-out

The number of turns made by an aircraft taxiing on the ground was expected to affect the fuel burn. One reason is because the aircraft may slow down during its turn and have to speed up again after completing it, and the other reason might be the use of differential thrust for turning. A 'turn' was defined to be a heading change of at least 30 degrees, that was held over at least 30 seconds. Figure 5-2 shows the heading variation during taxi-out for a sample flight. Each time instant was tagged by a binary flag representing detection, or otherwise, of a turn in progress. Each set of contiguous non-zero flags was counted as one turn. The results from automatic detection were compared with visual inspection across several flights and were found to correctly count the number of turns in almost all cases.

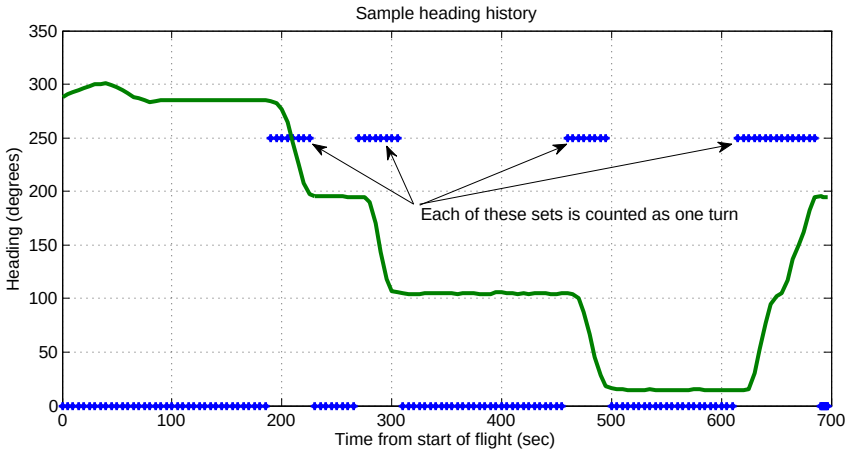

Figure 5-2: Plot of heading history for one flight

Detection of number of stops during taxi-out

The number of stops made by an aircraft was also expected to be a determinant of fuel burn, because of the throttle adjustments necessary during the stop-go event. Usually, an aircraft has to stop during a handoff from one ground controller to another, because there is passing traffic on an intersecting taxiway/runway, or in the runway departure queue. There are two ways in which an aircraft can be brought to a halt: one way is to apply the brakes while reducing the thrust to idle, and the other is to apply the brakes while keeping the thrust constant. There are fuel burn tradeoffs involved with both methods. Reduction of the thrust while stopping reduces fuel consumption if the duration of the stop is long. However, thrust has to be increased to start taxiing again (*breakaway power*), and this is accompanied by a spike in the fuel consumption. Also, aircraft engines exhibit some time lag while spooling up, leading to slow response times when starting from a standstill. On the other hand, if the aircraft is stopped using only the brakes, fuel flow rate remains high, and can lead to significantly higher total fuel burn if the stop is prolonged. However, there is a performance benefit on restart as previously outlined. Consequently, pilots tend to use one of the two methods depending on personal preference and operational considerations. In this study, an aircraft was defined to have stopped during its taxi phase if its velocity dropped and stayed below a *stop threshold* of 2.25 m/s for at least 20 seconds, and then subsequently increased above a *start threshold* of 6.25 m/s. The results from the stop detection algorithm are shown in Figures 5-3 and 5-4 for two sample cases. Note that event logging takes place only if the aircraft has already taxiing, which means that the initial start is not counted.

5.3 Estimation of Taxi-out Fuel

Having extracted the different taxi phases, we now investigate two possible linear regression models that estimate the fuel burn (normalized by absolute temperature) as a function of different independent variables.

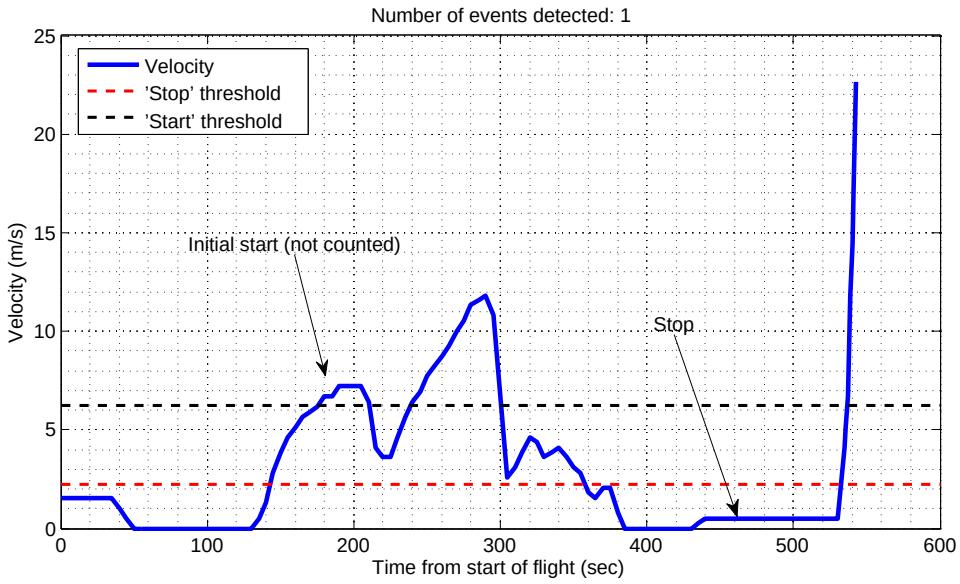

Figure 5-3: Flight with a single stop

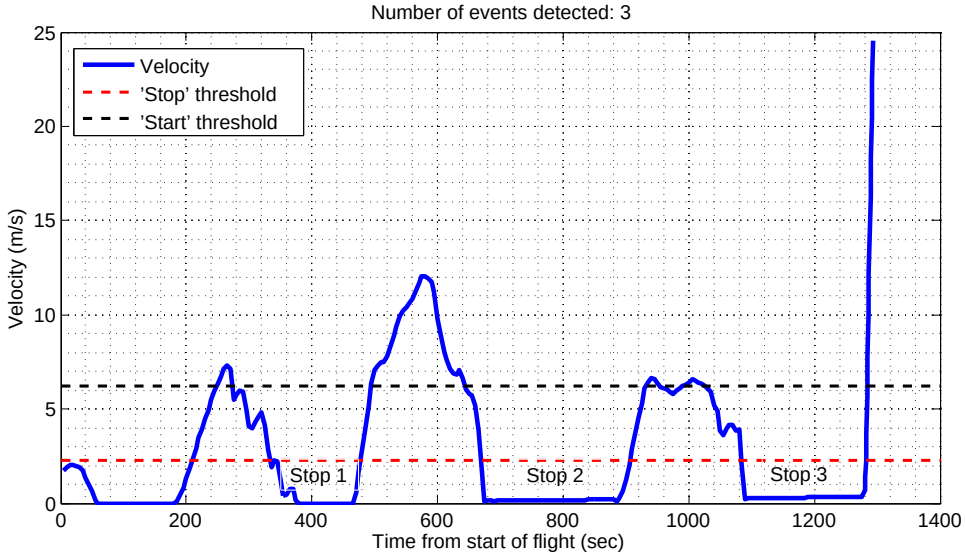

Figure 5-4: Flight with three stops

5.3.1 Model 1: Taxi time, number of stops and number of turns as independent variables

Formulation: Model 1

According to our initial hypothesis, total fuel burn on the ground would be a function of the taxi time, number of stops and number of turns made by the aircraft. It is easy to see that taxi time would be a determinant of fuel burn. In addition, given that the engines run at constant thrust for a large part of the taxi-out process, we would expect the effect of taxi time on fuel burn to be linear. Stops were expected to affect fuel burn because of the breakaway thrust required to start moving once an aircraft was stopped. This should add a relatively fixed fuel penalty per stop, resulting in a linear effect of the number of stops on fuel burn. Similarly, turns would require some adjustment of the power setting, but assuming that the adjustment would be similar for each turn, this effect should also be approximately linear. Finally, we know from available literature [34, 35] that engine sfc (specific fuel consumption) is proportional to the square root of ambient temperature. Therefore, we normalized for the effect of ambient temperature experienced by each flight, by formulating the regression as follows:

$$\frac{f}{\sqrt{T_{amb}}} = a_1 + b_1 \cdot t + c_1 \cdot n_s + d_1 \cdot n_t \tag{5.1}$$

Here, f is the total fuel consumed, t is the total taxi time, n_s is the number of stops, and n_t is the number of turns made by the aircraft during taxi. The quantities a_1, b_1, c_1 and d_1 are the parameters to be estimated. The coefficient b_1 will be the baseline fuel consumption rate of that aircraft type during taxi. Note that actual variation of temperature in the available data was only 17 K, which would not significantly impact the regression results, even if we had not normalized the fuel burn by ambient temperature.

Type	Constant		Taxi Time		# Stops		# Turns		Corr.	St. Dv.
	a_1 (kg/K$^{0.5}$)	p_{a1}	b_1 (kg/s-K$^{0.5}$)	p_{b1}	c_1 (kg/K$^{0.5}$)	p_{c1}	d_1 (kg/K$^{0.5}$)	p_{d1}	ρ	σ (kg/K$^{0.5}$)
A319	-0.01	0.94	0.0124	0	-0.01	0.82	-0.02	0.48	.99	7.82
A320	-0.26	0.05	0.0125	0	0.1	0.1	-0.02	0.31	.99	9.8
A321	-0.19	0.19	0.0133	0	0.15	0	-0.05	0.03	.99	7.34
A330-202	0.98	0	0.0192	0	0.94	0	-0.02	0.8	.97	19.29
A330-243	-1.6	0	0.0265	0	0.24	0	0.09	0.01	.99	12.15
A340-500	-1.56	0	0.0371	0	0.25	0.27	0.07	0.46	.99	38.31
ARJ85	-0.28	0	0.0103	0	0.08	0.02	0.01	0.28	.99	4.67
B757	0.24	0.18	0.0175	0	0.19	0.06	-0.1	0.02	.98	9.58
B767	-0.22	0.48	0.0178	0	0.73	0	0.15	0.01	.95	23.32
B777	-1.71	0	0.0338	0	0.19	0	-0.01	0.8	.99	11.54

Table 5.3: Regression Results: Number of Stops and Turns

Results: Model 1

Table 5.3 lists the results of the parameter estimates calculated using least-squares regression. The estimates are accompanied by corresponding statistical p-values. A threshold of 0.1 was assumed for inferring statistical significance of each variable, *i.e.*, variables with p-values below 0.1 are assumed to be statistically significant. The aircraft types for which one or more of the variables are statistically insignificant have been highlighted. Note that some outliers with unusually long taxi times were ignored in the estimation procedure. There are no more than one or two of such points for any single type of aircraft, constituting approximately 0.5% of all data. Note also that the parameters a_1, c_1 and d_1 have units of kg/K$^{0.5}$, while parameter b_1 has units of kg/s-K$^{0.5}$. In fact, b_1 should correspond to the fuel burn index for the aircraft type, multiplied by the number of engines and divided by the square root of ambient temperature. A comparison with Figure 5-1 shows that this is indeed the case. Some important points to note, regarding Table 5.3, are listed below:

- p-values for the parameter b_1 are uniformly zero, which means that taxi time is certainly a determinant of fuel consumption. This was, of course, expected. It also contributes the most to total fuel consumed.

- The statistical significance of the number of stops depends on the aircraft type. Some types show a definite relationship, while others show almost none.

- The coefficients of the number of turns are very small, even in comparison with the coefficients of number of stops. Given the dominance of taxi time in the

regression, the effect of turns on fuel burn can be said to be negligible.

- The statistical significance of the number of turns also depends on aircraft type. In addition, the significance of stops and turns does not appear to be related.

- ρ is the correlation coefficient between the estimated fuel burn and the actual fuel burn. These values are uniformly high.

- σ is the corresponding standard deviation of the residuals. Note that the reason that some of these values are larger than others is because the aircraft themselves are large (Table 5.1), which means that the total fuel consumed is more as well. The ratio of σ to average total fuel consumed is more or less the same for all types of aircraft.

Variability in statistical significance of stops and turns

The differences in p-values across aircraft types led to an investigation of the stopping process in more detail. As seen from Figures 5-5 and 5-6, a start from having stopped was accompanied by a spike in fuel consumption in some cases, and by none in other cases. This variation was noticed between flights of the same aircraft type, across different aircraft types, and sometimes even within two different stop events on the same flight. No common characteristic was found to explain this difference across aircraft types. Possible factors considered were aircraft size, engine manufacturers, locations of operating airports, aircraft weight class and period of initial introduction of the aircraft. However, when considering the thrust setting profile, we found that acceleration events after stops that were not accompanied by an increase in the fuel burn rate, were not accompanied by a change in thrust setting either. Therefore, the logical conclusion was that the difference in results was due to differences in pilot behavior (whether reduction of thrust when stopping was more or less prevalent for the given aircraft type). A similar argument would hold true for thrust characterization during turns. Since the aim was to model the effect of stops as executed by the *average* pilot, specific reasons for this variation were not investigated.

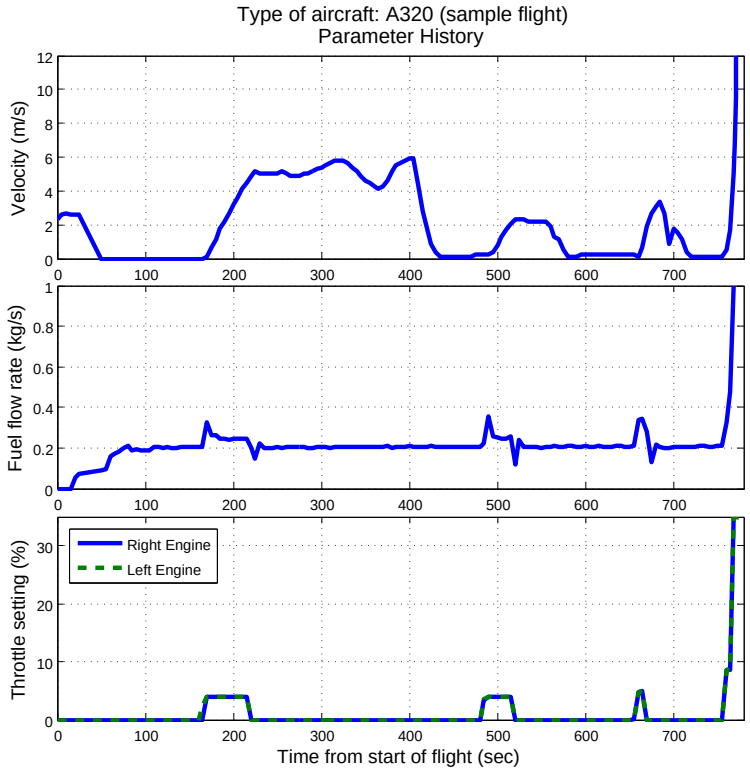

Figure 5-5: Simultaneous plot of velocity, fuel consumption rate and engine thrust settings for an Airbus A320: Increase in velocity (after stops) accompanied by spikes in fuel flow rate

5.3.2 Model 2: Taxi time and number of acceleration events as independent variables

Formulation: Model 2

The model discussed previously produced good estimates of the total fuel burn, as seen from the values of the standard deviation of residuals. However, the differences in statistical significance of the explanatory variables suggested that other factors might be more important determinants of fuel burn. Therefore, it was decided to drop the number of stops and number of turns from the regression, and instead add the number of acceleration events as an independent variable. The logic behind this decision was that fuel flow rates were seen to increase for aggressive starts from standstill, as

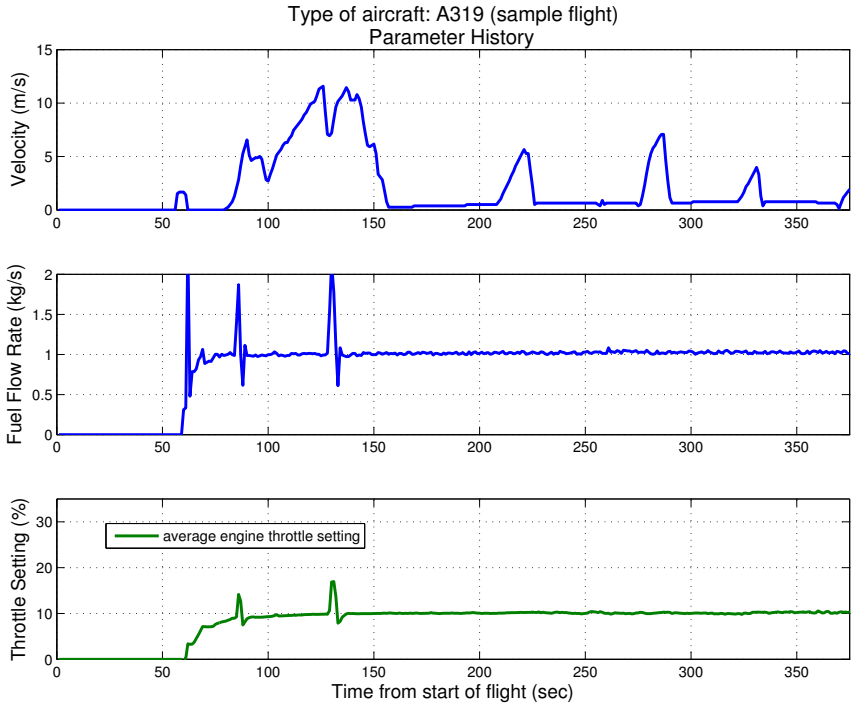

Figure 5-6: Simultaneous plot of velocity, fuel consumption rate and engine thrust settings for an Airbus 319: No change in fuel flow rate during acceleration from some stop events.

opposed to gradual ones. An acceleration event was logged if the aircraft accelerated at more than 0.15 m/s^2 for at least 5 seconds. In Equation (5.2), n_a is the number of acceleration events. The other variables have the same definition as before.

$$\frac{f}{\sqrt{T_{amb}}} = a_2 + b_2 \cdot t + c_2 \cdot n_a \tag{5.2}$$

Results: Model 2

The results from parameter estimation for Model 2 have been listed in Table 5.4. It is seen that both independent variables are statistically significant for all aircraft types but one. Even for the Boeing 757, the p-value for the number of acceleration events is not very large. Comparing the results with those from Table 5.3, we can also see that the correlation coefficients are higher and the standard deviation of residuals is consistently lower for Model 2. Figures 5-7 and 5-8 compare the fuel burn estimates

Type	Constant		Taxi Time		# Acc. Events		Corr.	Std. Dev.
	a_2 (kg/K$^{0.5}$)	p_{a2}	b_2 (kg/s-K$^{0.5}$)	p_{b2}	c_2 (kg/K$^{0.5}$)	p_{c2}	ρ	σ (kg/K$^{0.5}$)
A319	0.0811	0.31	0.0122	0.0	0.0965	0.0004	0.9938	6.85
A320	-0.0896	0.24	0.0124	0.0	0.1174	0.0000	0.9924	8.90
A321	0.0942	0.37	0.0129	0.0	0.0832	0.0184	0.9858	8.14
A330-202	0.2904	0.02	0.0217	0.0	0.3809	0.0001	0.9816	14.44
A330-243	-0.0903	0.25	0.0265	0.0	0.1007	0.0312	0.9965	9.12
A340-500	0.3626	0.10	0.0375	0.0	0.3984	0.0137	0.9918	30.59
ARJ85	0.0973	0.00	0.0102	0.0	0.0366	0.0203	0.9928	4.12
B757	0.2133	0.03	0.0173	0.0	0.0699	0.2007	0.9861	8.83
B767	0.1584	0.20	0.0202	0.0	0.1929	0.0012	0.9795	16.50
B777	-0.1223	0.02	0.0335	0.0	0.1385	0.0093	0.9985	8.75

Table 5.4: Regression Results: Acceleration events

to actual burn for two aircraft types. It is clear that the prediction accuracy of Model 2 is very good. Figure 5-9 shows a scatter plot of the residuals for the Boeing 777. The whiteness of these residuals was tested by calculating the autocorrelation of the residuals vector within each aircraft type [8, 9]. A sample plot of the result is shown in Figure 5-10. It is quite clear that the residuals are white, which means that optimal use of the information in the dataset has been made.

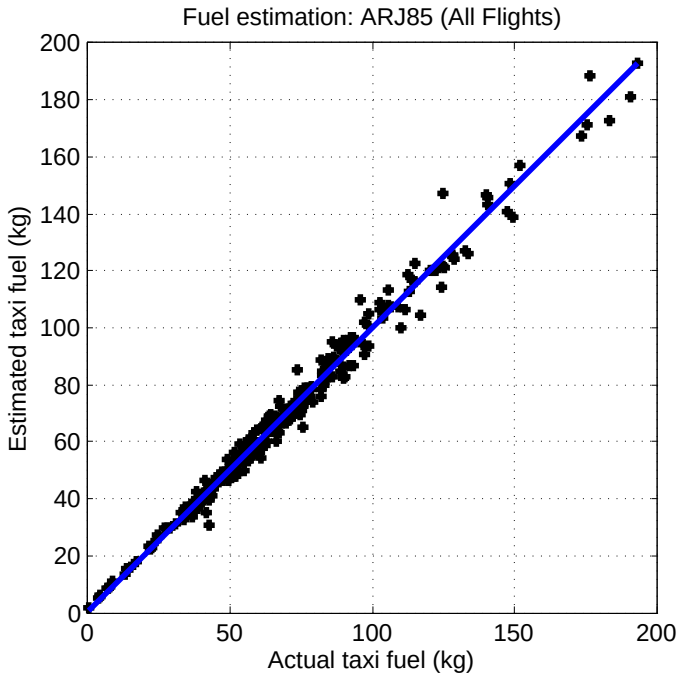

Figure 5-7: Regression for the Avro-RJ 85 using number of acceleration events

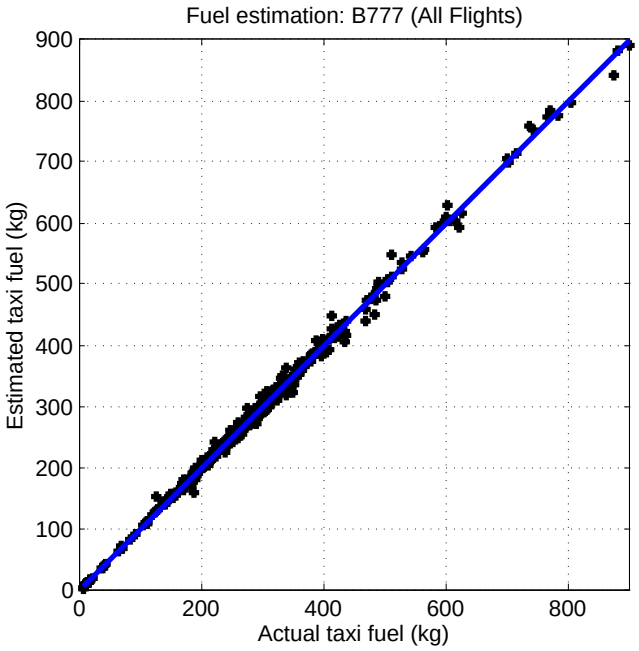

Figure 5-8: Regression for the Boeing 777 using number of acceleration events

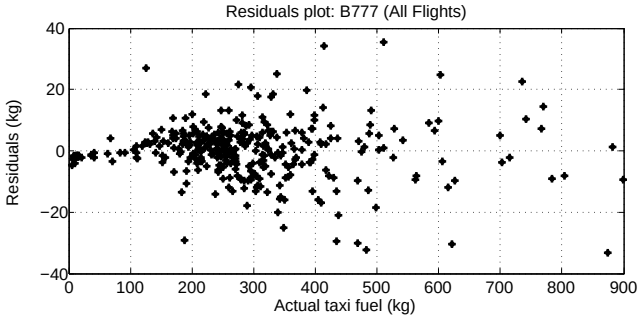

Figure 5-9: Residuals from the estimation of fuel consumption for the B777

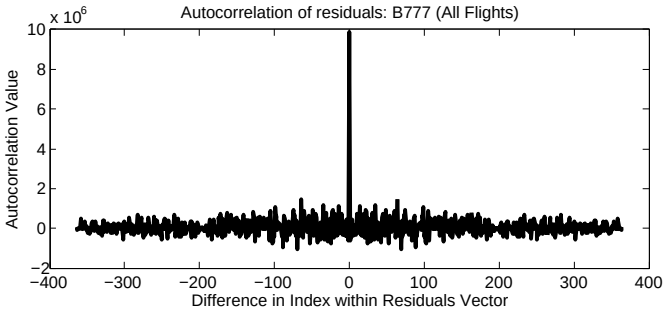

Figure 5-10: Autocorrelation of residuals for the B777

5.4 Summary

5.4.1 Discussion of results

The two regression models for taxi-out fuel burn provide us with several interesting results. The first one is that the total taxi time is by far the main driver of fuel consumption. In other words, an accurate estimate of the fuel burn index along with the taxi time can provide a reasonably accurate estimate of the fuel consumption of a surface trajectory. The analysis also shows that for some of the aircraft types studied, the ICAO engine databank overestimates the fuel burn indices.

The FDR analysis also suggests that contrary to assumptions made in prior studies [2], stops or turns by themselves may not necessarily result in an increase in fuel burn rate, and therefore do not contribute much information beyond the total taxi time. This can be explained by the variability in pilot behavior (since there may not be significant thrust changes accompanying stops or turns), the inherent variability in the thrust settings during taxi (which may be significantly different from the ICAO 7% assumption), and the dominance of the total taxi time as a driver of taxi fuel burn. However, acceleration events (defined as the aircraft accelerating at more than 0.15 m/s^2 for at least 5 seconds) have a small but statistically significant impact on the taxi fuel burn. The inclusion of these effects will provide a more accurate estimate of surface fuel consumption, and will also need to be considered in surface traffic flow optimization.

Chapter 6

Estimation of Surface Trajectory Fuel Burn

6.1 Introduction

It was indicated in Section 5.1.1 that the fuel burn model developed using FDR data can be used to estimate the fuel burn associated with surface surveillance flight tracks. Since ASDE-X data contains all the information required to populate the right-hand side of Equation (5.2), it is possible to associate a fuel consumption estimate with each detected flight. This process is most useful when applied to departures, as it can then be used to quantify expected benefits from congestion-mitigation strategies. While post-analysis of the costs and benefits of such strategies is useful, a predictive measure of expected fuel-burn savings would be even more valuable. An initial idea to carry out such an exercise is also described in this chapter.

6.2 Fuel Burn Estimates from ASDE-X Tracks

One of the challenges involved with estimation of fuel burn for a host of ASDE-X trajectories is that there are bound to be some aircraft and engine types which are not available in the FDR data. In such instances, exact estimates of fuel burn cannot be obtained. To obtain approximate estimates, it is assumed that the coefficients

estimated for one aircraft and engine type are valid for other similar aircraft/engine combinations not available in the FDR data.

As an illustrative example of the fuel burn estimation procedure, consider Figure 6-1, which shows a track obtained from the ASDE-X equipment at Boston Logan International Airport. The aircraft type was the Boeing 767-300. Figure 6-2 shows the corresponding velocity-time chart. The methodology from Model 2 (Section 5.3.2) when applied here, indicates that the total taxi time was 840 seconds, and that the flight experienced two 'acceleration events'. From historical weather data [36], the mean ambient temperature at Boston Logan on the day of this flight (Nov 24, 2010) was 279K. Looking up the fuel burn coefficients for the B767 from Table 5.4, the taxi-out fuel burn for this flight may be estimated from Equation (5.2) as follows:

$$\frac{f}{\sqrt{297}} = 0.1584 + 0.0202 \cdot 840 + 0.1929 \cdot 2 \implies f = 292.5 \quad \text{kg}$$

Figure 6-1: Sample ASDE-X flight track from Nov 24, 2010

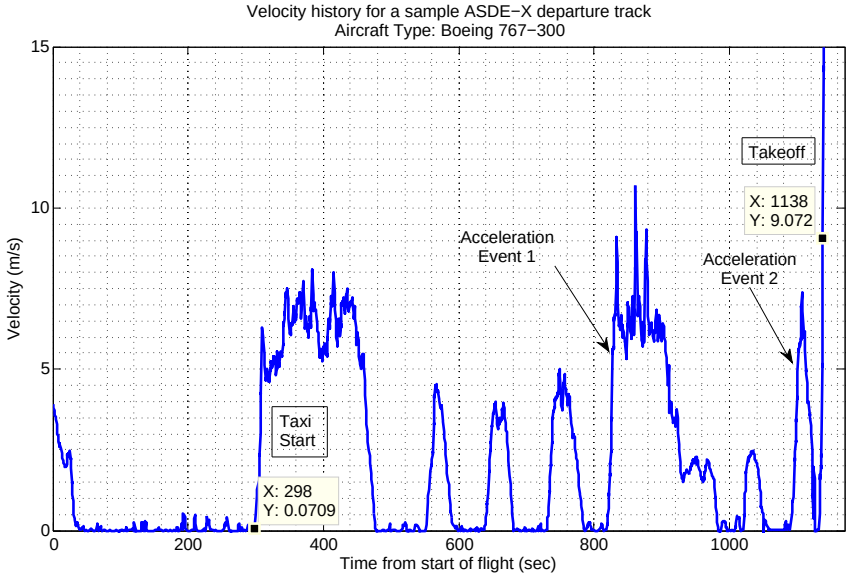

Figure 6-2: Velocity history for sample flight track

6.3 Fuel Burn Prediction

In order to estimate the potential fuel burn benefits from congestion mitigation strategies, the independent variables in Equation (5.2) need to be estimated. The total taxi-out time may be estimated using methods such as those described in Chapter 4. To estimate the number of acceleration events, we need some way of relating the level of surface traffic to the expected number of acceleration events. The following discussion is limited to behavior in the departure queue, since a reduction in queue size is an important objective for most congestion control methods. A similar analysis may be carried out for the entire taxi-out path.

Figure 6-3 shows the empirical variation of the average number of acceleration events encountering by a departing aircraft. The results are from Boston Logan. The X axis is composed of the departure queue size encountered by each aircraft. As seen in the figure, the number of acceleration events increase approximately linearly with the queue size, at the rate of 0.4 events for each additional aircraft in queue. The

Table 6.1: Summary: Regression from departure queue size to number of acceleration events in queue

Runway	Intercept	Slope
All	0.56	0.44
15R	0.63	0.37
22L	0.87	0.75
22R	0.64	0.36
27	0.25	0.60
33L	0.45	0.61

nonlinearity in the latter part of the plot corresponds to very few observations, as seen from the lower plot. We note that the slope of the line is less than 1, which means that an increase in queue size does not relate to an increase in acceleration events in the same proportion. This is a significant fact to consider when designing strategies that try to control the queue size. Similar behavior corresponding to departure queues for a single runway have also been seen. Figures 6-4 and 6-5 show the results for two specific runways, while Table 6.1 lists the values for all runways at Boston. Note that different runways may have different slopes. It is interesting to note that departures from runways 27 and 33L, which involve an active runway crossing, have a slope of 0.6 acceleration events for each additional aircraft in queue. On the other hand, departures from runways 15R and 22R, which do not involve active runway crossings, have a slope of 0.36. Runway 22L is not often used for departures, and usually only handles aircraft that have requested it specifically (it is longer than 22R) or have a controlled departure time.

Were we to do benefits assessment for a strategy to control departure queue size, we could use this data to estimate the potential reduction of fuel burn. On average, a unit reduction in the departure queue size seen by an aircraft at BOS would reduce its acceleration events by 0.44, which would translate to a proportional reduction in fuel burn. Exact values would depend on the fleet mix (Table 5.4). In this way, the total fuel savings could be calculated. Note that the current analysis would be an estimate of the benefits accrued in the departure queue only. A similar method could be applied to look at benefits on the surface in general.

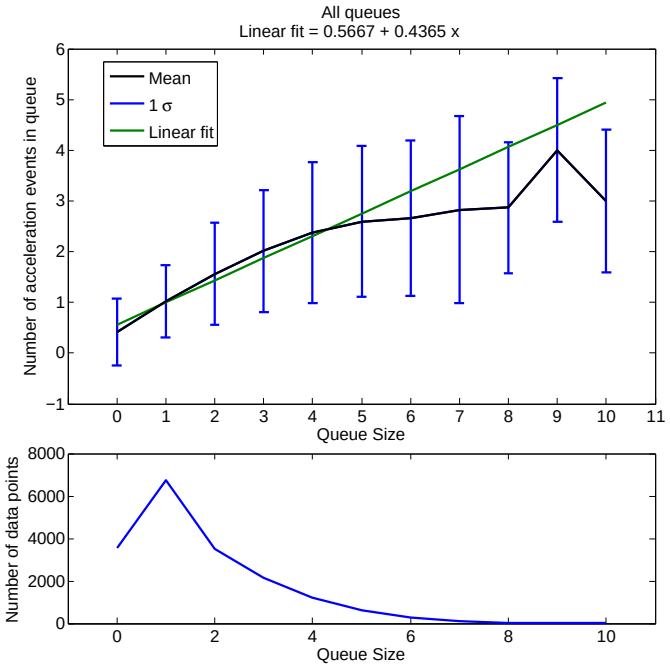

Figure 6-3: Regression from departure queue size to number of acceleration events in the queue (includes all queues)

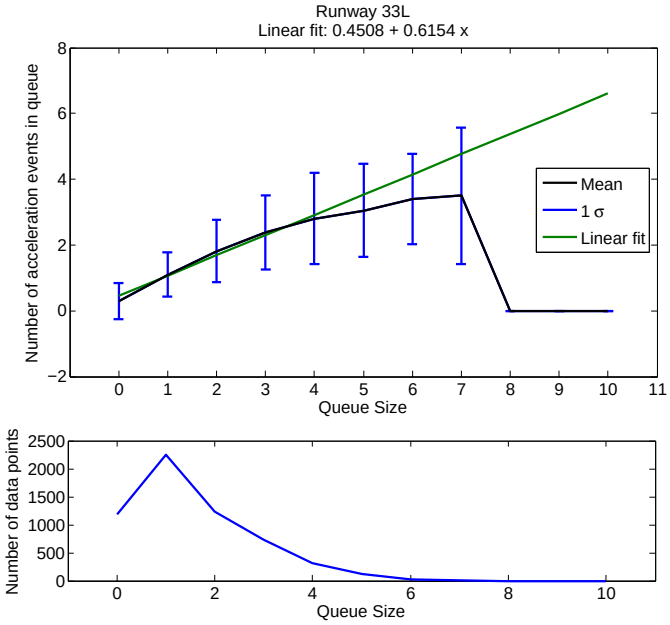

Figure 6-4: Regression from departure queue size to number of acceleration events in the queue (departures from Runway 33L)

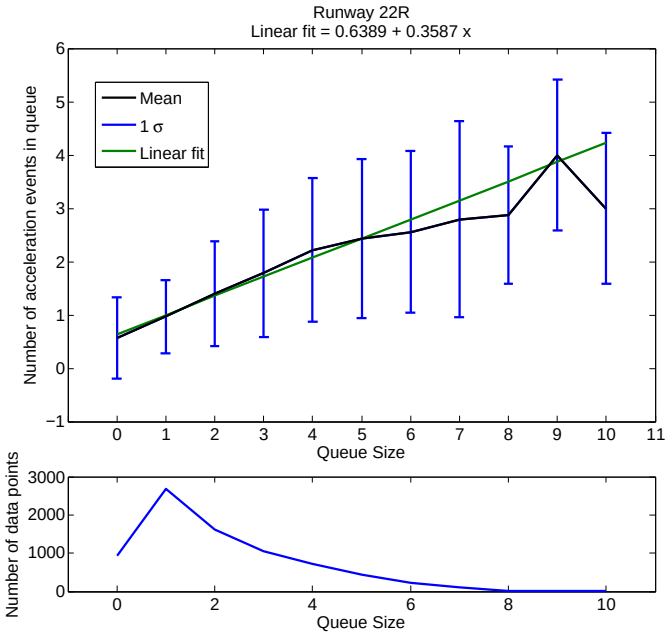

Figure 6-5: Regression from departure queue size to number of acceleration events in the queue (departures from Runway 22R)

6.4 Summary

In this chapter, the model developed in Section 5.3.2 was applied to estimation of fuel burn of ASDE-X aircraft trajectories. It was shown that the post-hoc estimation procedure is quite straightforward. Finally, a methodology that can be used to produce first order benefit estimates from congestion reduction was proposed.

Chapter 7

Conclusions

This thesis gradually developed a framework for analysis of airport surface operations. The process for filtering out the noise in surveillance data was described, which included automatic classification of aircraft taxi mode (straight, turning, stopped, etc.). This was followed by a description of current operations at Boston Logan International Airport, using directly measurable quantities such as queue size and also performance metrics such as average taxi-out times, runway utilization and departure spacing efficiency. It was shown that the performance metrics as defined in consultation with the Air Traffic Manager at BOS could be used to gain insights into potential areas of improvement.

This was followed by a probabilistic treatment of taxi-out time predictions. A network model of the airport surface was developed, with travel times over the network links modeled as random variables. The distribution of taxi times over these links was derived, and it was shown to be an accurate predictor for taxi-out times in an independent test data set. A simple algorithm used to predict taxi-out times for each aircraft was described, which uses the current state of traffic on the surface for improved estimation. The accuracy obtained by this method was shown to be better than that found in available literature, which is based on queuing theory and regression models. Finally, a procedure for estimation of taxi-out fuel consumption of each aircraft was described. Actual Flight Data Recorder data was used to tune the model, thus giving superior results as compared to the standard method recommended

by the International Civil Aviation Organization. A simple method that could be used to calculate the total surface fuel burn at an airport, along with potential benefits from reduced congestion, was described.

Currently, the taxi-out time prediction model is being improved with a view to obtain even greater accuracy. Specifically, ways to use more than the first moment of the distribution are being explored. The final objective is to use the insights from Chapter 3, combined with the prediction model in Chapter 4 and the fuel burn model in Chapter 5, to develop a framework for producing optimal pushback times and taxi-out paths for each aircraft.

Bibliography

[1] Sensis Corporation, East Syracuse, NY. *ASDE-X Brochure - ASDE-X 10/05.qxd*, 2008.

[2] Y. Jung. Fuel consumption and emissions from airport taxi operations. NASA Green Aviation Summit, 2010.

[3] R. Jordan, M. Ishutkina, and T. Reynolds. A Statistical Learning Approach to the Modeling of Aircraft Taxi Time. In *Digital Avionics Systems Conference*, Salt Lake City, UT, October 2010.

[4] E. Wan and R. van der Merwe. The Unscented Kalman Filter for Nonlinear Estimation. In *Symposium 2000 on Adaptive Systems for Signal Processing, Communication and Control*, Alberta, Canada, 2000. IEEE.

[5] S. Julier and J. Uhlmann. A New Extension of the Kalman Filter to Nonlinear Systems. In *AeroSense: 11th International Symposium of Aerospace/Defense Sensing, Simulation and Controls*, 1997.

[6] M. Grewal and A. Andrews. *Kalman Filtering: Theory and Practice using MATLAB*. John Wiley & Sons, Inc., 2nd edition, 2001.

[7] N. Bellotto and H. Hu. A Bank of Unscented Kalman Filters for Multimodal Human Perception with Mobile Service Robots. *International Journal of Social Robotics*, 2, Number 2, 2010.

[8] J. Durbin and G. Watson. Testing for Serial Correlation in Least Squares Regression I. *Biometrika*, 37:409–428, 1950.

[9] J. Durbin and G. Watson. Testing for Serial Correlation in Least Squares Regression II. *Biometrika*, 38:159–178, 1951.

[10] H. Idris, B. Delcaire, I. Anagnostakis, W. Hall, N. Pujet, E. Feron, R. J. Hansman, J-P. Clarke, and A. Odoni. Identification of flow constraint and control points in departure operations at airport systems. In *AIAA Guidance, Navigation and Control Conference*, August 1998.

[11] E. Pels, P. Nijkamp, and P. Rietveld. Inefficiencies and Scale Economies of European Airport Operations. *Transportation Research Part E*, 39, Issue 5, September 2003.

[12] D. Gillen and A. Lall. Developing Measures of Airport Productivity and Performance: an Application of Data Envelopment Analysis. *Transportation Research Part E*, 33, Issue 4, December 1997.

[13] E. Gilbo. Airport Capacity: Representation, Estimation, Optimization. *IEEE Transactions on Control Systems Technology*, 1, no.3, September 1993.

[14] V. Ramanujam and H. Balakrishnan. Estimation of Arrival-Departure Capacity Tradeoffs in Multi-Airport Systems. In *Proceedings of the 48th IEEE Conference on Decision and Control*, December 2009.

[15] Aviation system performance metrics database. `http://aspm.faa.gov/main/aspm.asp`, Federal Aviation Organization.

[16] N. Pujet, B. Delcaire, and E. Feron. Input-output modeling and control of the departure process of congested airports. *AIAA Guidance, Navigation, and Control Conference and Exhibit, Portland, OR*, pages 1835–1852, 1999.

[17] I. Simaiakis and H. Balakrishnan. Queuing Models of Airport Departure Processes for Emissions Reduction. In *AIAA Guidance, Navigation and Control Conference and Exhibit*, August 2009.

[18] I. Simaiakis and H. Balakrishnan. Impact of Congestion on Taxi Times, Fuel Burn and Emissions at Major Airports. *Transportation Research Record: Journal of the Transportation Research Board*, No. 2184, December 2010.

[19] R. de Neufville and A. Odoni. *Airport Systems: Planning, Design, and Management*. McGraw-Hill, 2003.

[20] Federal Aviation Administration. *Pilot and Air Traffic Controller Guide to Wake Turbulence*.

[21] P. Balakrishna, R. Ganesan, and L. Sherry. Accuracy of Reinforcement Learning Algorithms for Predicting Aircraft Taxi-out Times: A Case-Study of Tampa Bay Departures. *Transportation Research Part C*, 18, Issue 6, December 2010.

[22] J. Legge and B. Levy. Departure Taxi Time Predictions using ASDE-X Surveillance Data. In *26th International Congress of the Aeronautical Sciences*, 2008.

[23] H. Idris, J-P. Clarke, R. Bhuva, and L. Kang. Queueing Model for Taxi-out Time Estimation. *ATC Quarterly*, September 2001.

[24] P. Moertl, S. Atkins, J.M. Hitt, C. Brinton, and D. Walton. Factors for Predicting Airport Surface Characteristics and Prediction Accuracy of the Surface Management System. In *IEEE International Conference on Systems, Man and Cybernetics*, 2003.

[25] E. Nikolova, M. Brand, and D. Karger. Optimal Route Planning under Uncertainty. In *International Conference on Automated Planning and Scheduling*, Lake District, England, June 2006.

[26] E. Nikolova and D. Karger. Route Planning under Uncertainty: The Canadian Traveller Problem. In *Twenty-Third Conference on Artificial Intelligence*, Chicago, IL, July 2008.

[27] S. Kullback. *Information Theory and Statistics*. John Wiley and Sons, NY, 1959.

[28] B. Collins. Estimation of Aircraft Fuel Consumption. *Journal of Aircraft*, 19, No. 11:969–975, Nov. 1982.

[29] International Civil Aviation Organization. *International Standards and Recommended Practices, Annex 16, Environmental Protection: Aircraft Engine Emissions*, volume 2. Montreal, 3rd edition, 2008.

[30] Intergovernmental Panel on Climate Change (IPCC). *Aviation and the Global Atmosphere*. Cambridge University Press, 1999.

[31] D. Senzig, G. Fleming, and R. Iovinelli. Modeling of Terminal-Area Airplane Fuel Consumption. *Journal of Aircraft*, 46 No. 4, 2009.

[32] J. Patterson, G. Noel, D. Senzig, C. Roof, and G. Fleming. Analysis of Departure and Arrival Profiles Using Real-Time Aircraft Data. *Journal of Aircraft*, 46 No. 4, 2009.

[33] ICAO Engine Emissions Databank. `http://www.caa.co.uk/default.aspx?catid=702&pagetype=90`. [Retrieved December 2010].

[34] P. Hill and C. Peterson. *Mechanics and Thermodynamics of Propulsion*. Addison-Wesley, 2nd edition, 1992.

[35] T. Yoder. Development of Aircraft Fuel Burn Modeling Techniques with Applications to Global Emissions Modeling and Assessment of the Benefits of Reduced Vertical Separation Minimums. Master's thesis, Massachusetts Institute of Technology, 2007.

[36] `http://www.weather.com/outlook/health/airquality/wxclimatology/daily/02128`.